# FUEL PROCESSING CATALYSIS FOR MICROCHANNEL APPLICATIONS:
# METHANOL STEAM REFORMING AND SELECTIVE CO METHANATION

By

ROBERT ALEXANDER DAGLE

A thesis submitted in partial fulfillment of
the requirements for the degree of

MASTER OF SCIENCE IN CHEMICAL ENGINEERING

WASHINGTON STATE UNIVERSITY
Department of Chemical Engineering

May 2005

To the Faculty of Washington State University:

      The members of the Committee appointed to examine the thesis of ROBERT ALEXANDER DAGLE find it satisfactory and recommend that it be accepted.

_____
Chair

_____

_____

_____

**Acknowledgments**

Work contained in this manuscript is a culmination of research performed over the past five years in an effort to provide catalysis support to various portable power programs at PNNL. The researched contained here is the result of not only the efforts of the author but by several co-workers who have advanced this work in varying degrees and roles. The majority of the members of catalyst team, led by Yong Wang, have contributed greatly. These members include Ya-Huei (Cathy) Chin, Jianli (John) Hu, Chunse (James) Cao, Guan-Guang (Gordon) Xia, Daniel (Dr. P) Palo, Jamie (Doc) Holladay, Evan Jones, and Yong Wang. The author would like to acknowledge the above mentioned people for their superb efforts. He would specifically like to thank Yong Wang who has provided the leadership for all these related activities and who has graciously offered to act as his thesis advisor.

While the author was involved with all that is contained in this manuscript, he contributed in varying roles to each area. The author was most engaged in driving the

technical focus in the following areas:  crystallite size studies for both the methanol steam

reforming and selective CO methanation reactions, and selective CO methanation

pretreatment and synthesis studies.  The author attempted to liberally reference areas of

work where others should take credit.

# FUEL PROCESSING CATALYSIS FOR MICROCHANNEL APPLICATIONS: METHANOL STEAM REFORMING AND SELECTIVE CO METHANATION

Abstract

by ROBERT ALEXANDER DAGLE, M.S. ChE
Washington State University
May 2005

Chair: Yong Wang

In agreement with previous works, Pd/ZnO catalysts have been demonstrated as being selective for the methanol steam reforming reaction, which is due to the unique nature of the PdZn alloy formation upon reduction conditions higher than >350C. The effects of crystallite size, use of high surface area alumina support, Pd:Zn ratio, and Pd loadings were shown to affect the activity and selectivity to the methanol steam reforming reaction. By using a 9%Pd/ZnO/Al2O3 catalyst, with a Pd:Zn ratio of 0.38, performance was found to be similar to that of a commercial CuZnAl catalyst. Unlike their CuZnAl counterpart, PdZnAl catalysts are stable at much higher temperatures, thus, the benefits of increased kinetics due to higher operating temperature are realized.

Selective CO methanation as a strategy for CO removal in micro fuel processing applications was investigated over Ru-based catalysts. Ru loading, pretreatment and reduction conditions, and choice of support were shown to affect catalyst activity, selectivity, and stability. Even operating at a space-hourly-velocity as high as of 13,500 $hr^{-1}$, a 3%Ru/Al$_2$O$_3$ catalyst was able to lower CO in a reformate to less than 100 ppm over a wide temperature range from 240$^{o}$C to 285 $^{o}$C, while keeping hydrogen consumption of <10%.

**Table of Contents**

**List of Tables**

## List of Figures

**Figure 1**. X-ray diffraction patterns of 16.7 wt% Pd/ZnO (a) fresh, calcined at 350 $^{\circ}$C, (b) fresh, calcined at 600 $^{\circ}$C, (c) calcined and evacuated under high vacuum at 600 $^{\circ}$C, (d) spent, after reaction up to 300 $^{\circ}$C, and (e) after TPR to 600 $^{\circ}$C, showing diffraction peaks of ZnO (triangle), PdO (open square), Pd (open circle), and PdZn (filled circle). Reaction conditions: 0.1925g catalyst, 100 ms contact time or 36 000 GHSV, $H_2O/C = 1.8$, 1 atm. TPR conditions are the same as Figure 2.

**Figure 2.** Methanol conversion temperature profile under steam reforming of methanol (a) and the corresponded CO selectivity (b) for 4.8 wt% (triangle), 9.0 wt% (circle), and 16.7 wt% Pd on ZnO (both filled and open square). For 16.7%Pd/ZnO, the conversion profiles were acquired after two separate reduction temperatures: reduction at 125 $^{\circ}$C (open square) and after reduction at 350 $^{\circ}$C (filled square). All other catalysts were tested after reduction at 350 $^{\circ}$C. Reaction conditions: 0.1925g catalyst, 100 ms contact time or 36000 GHSV, $H_2O/C = 1.8$ (molar), 1 atm.

**Figure 3:** a) Conversion and b) CO selectivity as a function of reaction temperature for the organically prepared series Pd/ZnO catalysts (GHSV=14,400 hr$^{-1}$, 1 atm, $H_2O/C=1.8$ (molar), $P_{N2}=0.25$atm)

**Figure 4:** a) Conversion and b) CO selectivity as a function of reduction temperature for the organically prepared series Pd/ZnO catalysts (GHSV=14,400 hr$^{-1}$, 275C, 1 atm, $H_2O/C=1.8$ (molar), $P_{N2}=0.25$atm).

**Figure 5:** High Resolution TEM on 10%Pd/ZnO after 425$^{\circ}$C reduction for a) an organically prepared catalyst and b) using aqueous preparation.

**Figure 6**: Expected crystallite size found from high resolution TEM as a function of CO selectivity (GHSV=14,400 hr$^{-1}$, 275$^{\circ}$C, 1 atm, $H_2O/C=1.8$ (molar), $P_{N2}=0.25$atm).

**Figure 7.** Methanol conversion and CO selectivity as functions of Pd/Zn ratio and Pd loading (260$^{\circ}$C, GHSV = 14,400 hr$^{-1}$, Steam/carbon =1.78).

**Figure 8:** CO selectivity as a function of feed steam/carbon ratio on 10%PdZnO/Al$_2$O$_3$ catalyst (GHSV=2100 hr$^{-1}$, 1 atm, 320$^{\circ}$C, methanol feed=0.27atm, water feed varied with N2 dilutent added to maintain constant GHSV for all runs).

**Figure 9:** CO selectivity as a function of temperature on 10%Pd/ZnO/Al$_2$O$_3$ catalyst (GHSV=2100 hr$^{-1}$, 1 atm, $H_2O/C=1.2$, $P_{N2}=0.4$ atm).

**Figure 10**: Effect of Ru metal loading and temperature on a) CO concentration in the effluent and b) $H_2$ consumption (approximate feed composition: 0.9%CO, 24.5%CO$_2$, 68.9%H$_2$, 5.7%H$_2$O, SV=13,500 hr$^{-1}$).

## 1. Introduction
## 1.1 Overview

As fuel cell research and development becomes a flourishing area in recent years, fuel processing including hydrogen generation, purification, and storage is drawing a great deal of attention. Fuel cell systems are being developed for several applications, including distributed and portable power generation and for consumer applications[1]. At Pacific Northwest National Laboratory (PNNL) much development has been done in the area of fuel processing for portable power generation using microchannel technology[2,3,4] Microchannel reactor architecture provides rapid and efficient heat transfer. Advanced catalysts utilized in these systems are tailored to take full advantage of the thermal properties of the reactors. The result is that fuel conversion processes that might normally have reactor residence times on the order of seconds, now have residence times on the order of 0.01-.0.10 seconds. Using this approach has enabled the development of fuel processing systems for portable power applications that are not only efficient but small and lightweight[2].

## 1.2 Fuel Processing Strategies

Typical fuel processing strategies include steam reforming, partial oxidation and – as a combination of these processes – autothermal reforming[5]. Both preferential oxidation and autothermal reformation introduce oxygen (air) into the system and burn with the reforming fuel to produce the heat required for the reforming reactions(s) to occur. In steam reforming, an external combustor is used to provide the heat. While each technology has advantages and disadvantages, steam reforming is usually used at PNNL because it offers the highest theoretical efficiency, and produces the highest hydrogen

1

composition[3]. The requirement of an external heat source can be addressed through the advanced heat and mass transfer provided by microreactors. All three reforming strategies, however, require additional removal of carbon monoxide since the current permeable membrane fuel cell (PEMFC) cannot operate with carbon monoxide levels higher than several ppm.

## 1.3 Methanol Steam Reformation

Among hydrocarbon fuels, methanol has been widely studied as a source of hydrogen production for the fuel cell due to its high hydrogen/carbon ratio, low sulfur content, and relatively low reforming temperature ($250^{o}C$-$350^{o}C$). Due to the high energy density of methanol (~5.6 kWh/kg compared to ~0.12 kWh/kg for lithium ion batteries), even a very inefficient chemical to electrical device could be a significant over the available secondary batter technology[4]. The methanol steam reforming reaction is shown in Eq (1). Three moles of hydrogen are produced for every mole of methanol reacted. The water-gas-shift reaction, shown in Eq (2) must be minimized to not only maximize hydrogen production but due to CO poisoning of the fuel cell. CO produced by steam reformation must be reduced to ppm levels before introduction to the fuel cell.

$$CH_3OH(g) + H_2O(g) = 3H_2(g) + CO_2(g), \ \Delta H^0 = 49.5 \ \text{kg/mol} \tag{1}$$

$$CO(g) + H_2O(g) = CO_2(g) + H_2(g), \ \Delta H^0 = -41 \ \text{kg/mol} \tag{2}$$
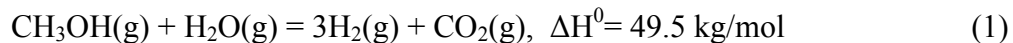
For portable power applications highly active and selective catalysts to $CO_2$ is desired. Faster kinetics results in higher throughputs and smaller devices[2].

Most research has focused on Cu-based catalysts which exhibit high activity and selectivity to $CO_2$ and $H_2$[4,9]. However, the Cu-based catalysts have significant disadvantages, including their pyrophoric nature, tendency to deactivate at high temperature $(>\sim280^oC)$[2,4]. In addition, stability under certain oxidizing environments is a concern[6]. Group VIII metals exhibit different performance than copper based catalysts. Over Group VIII metal catalysts, methanol decomposes to CO and $H_2$, shown in Eq (3).

$$CH_3OH(g ) = CO(g) + 2H_2(g),\ \Delta H^0 = 90.7\ kg/mol \qquad (3)$$
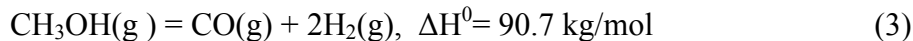
In the presence of water, the kinetically slower water-gas-shift reaction Eq (2) will occur, to a degree depending on the shift activity of the catalyst, thus shifting some of the $CO_2$ to CO. However, the significant amount of CO produced makes this an unattractive option.

Iwasa et. al was the first to report that Pd supported on ZnO and reduced at $>300^oC$ has exceptional high activity and selectivity to $CO_2$ and $H_2$[4,7]. Combined TPR, XRD, XPS, and TEM methods revealed the formation of a PdZn alloy under reduction conditions higher than $300^oC$[4,8,9]. It was shown that the reactions proceeded selectively towards methanol steam reforming over the catalysts having the alloy phase, whereas the catalysts having metallic phase exhibited poor selectivities to $CO_2$. Upon alloy formation, Iwasa's

group proposed a reaction mechanism markedly different than decomposition Eq (3), as with Group VIII metals alone, or one utilizing the water-gas-shift reaction Eq (2). Rather, the following mechanism, with a formic acid intermediate has been propsed[8]:

$$CH_3OH(g) = HCOH(g) + H_2(g)$$

$$HCOH(g) + H_2O(g) = HCOOH(g) + H_2(g) \qquad (4)$$

$$HCOOH(g) = CO_2(g) + H_2(g)$$
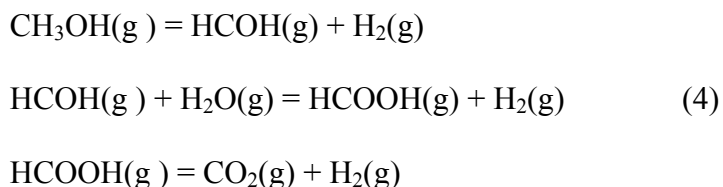
It has been argued that since this reaction does not include the decomposition of methanol to CO, and does not contain CO as an intermediate in the formation of $CO_2$, less-than equilibrium amounts of CO can be produced during steam reforming of methanol[2].

Studies in surface science has revealed that the structures of aldheydes absorbed on Cu is greatly different than that on Group VIII metals such as Pd[11]. In temperature desorption experiments, it was found that on Cu, these aldheydes absorb preferentially in $\eta^1(O)$-structure (the oxygen in the carbonyl, C=O, is bonded to the Cu surface maintaining its double bond). On Group VIII metals the aldehydes absorb as $\eta^2(CO)$-structure (the carbon loses its double bond and absorbs to the metal surface, as does the oxygen). Thus, on copper surfaces, the aldehyde preserves its molecular identity, whereas the on the Group VIII surfaces, the bonds are ruptured. Hence, it has been hypothesized that the difference in the original catalytic functions of copper and Group VIII metals for the steam reforming and dehydrogenation of methanol is ascribed to the difference in structures of the HCHO intermediates formed on these metals[11]. Furthermore, while the

mechanism on PdZn is not well understood, it has been hypothesized that based on similar performances, this phenomenon occurs on PdZn very similarly to that of Cu surfaces. Thus, the novel catalytic function typical of Cu emerges from PdZn systems as well.

Pd/ZnO based catalysts are selective to $CO_2$, are non-pyrophoric and do not produce methane below $400^oC$[2,4]. However, CuZnAl catalysts have still been shown to be more active for methanol steam reforming, therefore, for useful applications, PdZn has not yet been considered a viable option for fuel processing applications[8]. Also, some researchers have questioned the practicality of catalysts containing precious metals (Pd), compared to the base metal (Cu) catalysts, due to economic concerns[13]. However, in small, microscale applications where activity and robustness is essential, catalyst cost in not a primary concern[11].

## 1.4 CO Cleanup Options

Reforming of alkanes or higher alcohols is typically conducted at high temperatures, and requires the water-gas-shift step to reduce the CO concentration in the reformate to 1-2%[13]. On the other hand, reforming of methanol can be carried out at lower temperatures ($<350^oC$), which directly yields a CO concentration in the same range with no need for a water-gas-shift step[2]. Either way, further "deep removal" of CO to concentrations below 100 ppm for even the most CO tolerant fuel cell electrode catalysts is needed.

Three processes can be used to further reduce CO in the feed; preferential, or selective oxidation, methanation, and membrane separation[14].

*Preferential Oxidation*

Preferential oxidation catalytically oxidizes CO to $CO_2$. The reaction works well despite the presence of $H_2$ in the feed stream. Disadvantages include the complexity of precisely adding controlled amounts of oxygen (air) to the system to avoid $H_2$ oxidation [13]. Nonetheless, much focus in the literature has been on developing preferential oxidation catalysts which is considered by many to be the primary choice for the removal of CO from hydrogen-rich streams[15,16].

*Hydrogen Membranes*

Hydrogen permeable membranes, usually employing Pd-based membranes, separate hydrogen from the other components (i.e. CO, $CO_2$, $H_2O$). This purification system can be beneficial where pure $H_2$ is desired. The main problem with palladium membranes is that they require a high pressure differential, which takes a toll on overall system efficiency. Membrane durability and cost is also an issue[13].

*Selective CO Methanation*

Removal of CO by means of methanation has long been known as a possible strategy[13,14,16], but remains as a daunting challenge in the presence of $CO_2$[10]. CO methanation, shown in Eq (1), is highly exothermic. The methane produced will act as an inert dilutent and will thus not react in the fuel cell. A disadvantage is the hydrogen penalty. It can be seen from Eq (1) that for every mole of CO converted, three moles of $H_2$ are required. Furthermore, the undesirable reaction of $CO_2$ methanation (Eq (2)) is also highly exothermic and consumes four moles of $H_2$ for every mole of $CO_2$ reacted[6]. A second undesirable reaction is the reverse-water-gas-shift (RWGS) reaction (Eq (3)) that is favored at high temperatures and can shift $CO_2$ to CO. In order to minimize the forward reaction of Eq (3) the reaction temperature must be kept as low as possible. Thus, a catalyst with minimal shift and $CO_2$ methanation activity is desired

$$CO(g) + 3H_2(g) = CH_4(g) + H_2O(g), \ \Delta H^0 = -206 \ kg/mol \quad\quad (1)$$

$$CO_2(g) + 4H_2(g) = CH_4(g) + 2H_2O(g), \ \Delta H^0 = -165 \ kg/mol \quad\quad (2)$$

$$CO_2(g) + H_2(g) = CO(g) + H_2O(g), \ \Delta H^0 = 41 \ kg/mol \quad\quad (3)$$
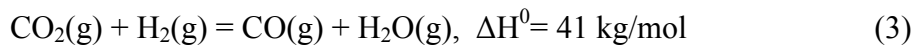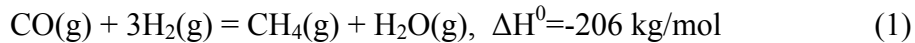
Methanation has the benefit of being a passive process, since it does not require any oxygen (air) addition, and it is only necessary to control the temperature[18]. However, the hydrogen consumption required for both the CO methanation and undesirable $CO_2$ methanation cuts into fuel efficiency. Thus, the general opinion is that methanation is not feasible at CO concentrations in the percent range[13,14]. Some have proposed using

selective methanation downstream from other CO removal processes, such as preferential

CO oxidation, for a cleanup process for the final 100ppm or so CO based on

methanation[13]. But selective methanation for use as a stand alone CO removal strategy

has not seriously been considered. As such, *most* of the research in this area has been

focusing on preferential CO oxidation and palladium membrane technology.

For a selective methanation strategy to be feasible, precise temperature control is critical.

Such process control is possible with the use of microchannel technology. Thus, at

PNNL, it is the use of microchannel technology, in conjuction with catalyst

improvements, that has recently lead to the exploration of selective CO methanation has a

viable, stand alone, carbon monoxide cleanup strategy.

## 1.5  Selective CO Methanation Catalysis

Carbon monoxide and carbon dioxide are pronounced catalyst poisons in many

hydrogenation reactions, including ammonia synthesis[17]. It is therefore necessary in

ammonia plants and most hydrogen plants to reduce the final amount of carbon oxides

remaining in process gas after the carbon dioxide removal stage to extremely low levels.

In almost all ammonia and hydrogen plants constructed since the 1960's the simple and

relatively inexpensive catalytic conversion of traces of carbon oxides to methane and

water has been used[17]. Therefore, the catalytic process of converting *both* carbon

monoxide and carbon dioxide has been widely established. However, the selective

methanation of carbon monoxide while limiting the methanation of carbon dioxide is a

more complex, less mature, technology.  Such a reaction scheme has not been previously required, except relatively recently for use in fuel cell applications.

Baker et al.[19] was among the first to utilize a *selective* CO methanation process, by using a ruthenium or rhodium on an alumina support catalyst to selectively hydrogenate carbon monoxide in the presence of carbon dioxide.  However, the CO feed concentration used, 0.29%, was considerably lower than the percent range needed for current applications as a stand alone process.  Additionally, relatively low feed flowrates from GHSV=500-2000 hr$^{-1}$ were reported.  Even with these lower flowrates the operating temperature ranges of only a few degrees on even the best catalyst, to maintain CO below 100 ppm, was probably too narrow to be applicable for actual devices applications.

Rehmat et. al. investigated this process at much higher space velocities of 9000-36,000 hr$^{-1}$ and higher temperatures of 125 $^{\circ}$C -300 $^{\circ}$C [20] with a similar feed as that of Baker et. al. (3000 ppm CO).  The higher space velocity tests did not yield CO outputs lower than 100 ppm.  While further catalyst performance enhancement was still desired, some useful insight into the reaction mechanism was observed.  In the absence of $CO_2$ the methanation reaction goes to almost completion at temperatures higher than that necessary to achieve the minimal CO output, when $CO_2$ is added (under similar space velocities).  Thus, it was suggested that while it is possible that for all the temperatures investigated the CO methanation reaction Eq (1) takes place along with the reverse shift reaction Eq (3), the latter is less noticeable up to an optimal temperature.  After reaching

this optimal temperature where the CO is lowest, the reverse shift reaction begins to predominate even the $CO_2$ methanation Eq (2) reaction.

Bohm et. al. described a process utilizing in part selective methanation using a Ru- and $TiO_2$- containing catalyst[21]. Van Keulen patented a two-stage, two-temperature range methanation process which utilized a Ru-based catalyst[22]. In a recent work by Otsuka et. al., several supports and metals were studied for CO methanation[23]. It was found that the effect of catalytic support could be explained by crystallite size. Catalytic activity of supported Ru catalysts for the complete removal of CO through methanation becomes higher as crystallite sizes of Ru become smaller[23]. The most promising catalysts – $Ni/ZrO_2$ and $Ru/TiO_2$ catalysts – were studied in the presence of $CO_2$. It was found that while these catalysts can reduce the CO output to levels below 100 ppm, undesirable $CO_2$ methanation Eq (3) occurs relatively quickly. For example, for the operating conditions reported, the methane output increased 4-fold in just $40^{o}C$, once the CO had reached <100ppm at $215^{o}C$[23].

Further catalyst improvements are required for selective CO methanation to be a viable option for fuel processing catalysis. In particular, more active catalysts are desired. Microreactors for steam reforming developed at PNNL are typically optimized to run at high throughputs from 10,000-60,000 $hr^{1}$ to maximize reactor efficiency. The ability of micro reactors to take full advantage of heat and mass transfer rates enables the use of highly active catalysts, yielding large throughputs. These highly active catalytic micro reactors are able to run at near isothermal conditions, with minimal adiabatic temperature

rises. For microchannel applications, catalysts are desired with fast kinetics, while exhibiting good selectivity, thus, minimizing undesirable $H_2$ consumption via $CO_2$ methanation.

## 1.6 Focus of this Work

A series of Pd/ZnO catalysts were prepared and the effects of the PdZn alloy formation on methanol steam reforming and CO selectivity were studied. Another series of Pd/ZnO catalysts were prepared and the effects of crystallite size were studied. To lower the temperature for methanol steam reforming or to reduce the reactor volume for the fuel processor, it is still highly desirable to increase the activity of Pd/ZnO catalysts. Activity enhancement has previously been found by increasing Pd loadings up to 10wt% and no further enhancements at Pd loadings higher than 10wt%[4,9]. A series of Pd/ZnO catalysts supported on high surface area and neutral alumina support with a surface area of 230m$^2$/g was investigated. The effects of Pd loading and Pd:Zn ratio of methanol steam reforming activity and CO selectivity were studied[4]. The effect of steam-to-carbon ratio and enhanced kinetics due to higher operating temperature are also discussed. Catalyst activity testing results and catalyst characterizations, including XRD, BET, and TEM, of the methanol steam reforming catalysts are included in this study.

For selective CO methanation to be a viable option for micro catalytic fuel processing devices, highly active, selective, and stable catalysts must be demonstrated. To achieve these objectives, we have studied the effects of metal loading, preparation method,

pretreatment conditions, reaction conditions, and choice of support on the performance of Ru-based catalysts for such applications.  Catalyst testing results and catalyst characterization using XRD and BET are discussed.


## 2. Experimental

### 2.1 Catalyst Preparation

*Methanol Steam Reforming Catalysts*

A series of Pd/ZnO catalysts were prepared from impregnating aqueous $Pd(NO_3)_2$ solution containing 20.19wt% Pd (Engelhard) onto ZnO powder (Aldrich, 99%) using a solution/solid ratio of 0.58ml/g[9].  The nominal Pd concentrations in the samples for the aqueous prepared samples are 4.8, 9.0, and 16.7wt%.  The impregnated samples were dried under vacuum at $110^oC$ for at least 8 hrs prior to calcining in air.  Unless otherwise noted thee calcinations was conducted under a 2C/min ramp followed by holding isothermally at 350C for 3hrs.  The organically prepared Pd/ZnO catlasyts were prepared using a Palladium II Acetate salt (Aldrich, 99.9%) using acetone as a solvent.  The same ZnO powder was used as those for the aqueous prepared samples.  Nominal Pd concentrations prepared are 0.5, 2.5, and 10%.  The same drying and calcination schedule was used as those for the aqueous prepared samples.  $Al_2O_3$ supported Pd-ZnO catalysts were prepared using one-step co-impregnation method[4]. Specifically, a concentrated palladium nitrate solution (20.19 wt% Pd, Engelhard Corp.) was mixed with $Zn(NO_3)_2 \bullet 6H_2O$ (99.5%, Aldrich) at $60^oC$.  A neutral $\gamma$-$Al_2O_3$ support (Engelhard Corp.) with a BET surface area of $230m^2/g$ was pre-calcined at $500^oC$ for 2 hrs and kept at $110^oC$ prior to the incipient-wetness impregnation step. The support was impregnated at

60°C with appropriate amount of the pre-mixed Pd and Zn nitrate solution to obtain the final products with various Pd loadings (1.2 to 15.7wt%) and Pd/Zn molar ratios (0.08 to 1.1). The wet sample was kept at 60°C for 1 hour before drying in air at 110°C overnight. The dried sample was then calcined at 350°C for 3 hours.

*Selective CO Methanation Catalysts*

Supported metal catalysts were prepared by a conventional impregnation method. A neutral γ-Al$_2$O$_3$ support (Engelhard Corp.) was pre-calcined at 500°C for 2hrs. A TiO$_2$ P25 extrudate (Degussa) was calcined at 700°C for 5 hrs. Zr(OH) powder (Aldrich) was calcined at 550°C for 3hrs to form ZrO$_2$. All supports were kept at 110°C prior to the incipient-wetness impregnation step. As a means to study the effect of crystallite size, dilute and concentrated solutions of ruthenium were used requiring multiple and single-step impregnations, respectively. For the multi-impregnations on alumina, zirconia, and titania supports, a ruthenium (II) nitrosyl nitrate solution (containing 1.5%Ru, Aldrich) was used. For the single impregnations on alumina support a concentrated ruthenium (III) nitrosyl nitrate solution (containing 9.9%Ru, Colonial Metals) was used. After each impregnation the wet sample was dried in air for at least 8 hour at 110°C. After the final impregnation and drying the sample was calcined at 350°C for 3 hours.
calcined at 350°C for 3 hours.

## 2.2 Catalyst Performance Evaluation

*Methanol Steam Reforming Catalysts*

Activity tests were carried out in a 4 mm I.D. quartz tube reactor. Approximately 0.200 g

of catalyst was loaded between two layers of quartz wool inside the reactor. A

thermocouple was placed in the middle of the catalyst bed. Unless otherwise mentioned,

a premixed mixture of $H_2O/C=1.8$ (molar) feed was introduced into the reactor by using a

syringe pump. The various feed rates are indicated for each test. Prior to entering the

reactor, the feed was fully vaporized through a vaporizer, operating at 200 $^o$C. Unless

otherwise mentioned, the catalysts were reduced *in-situ* under a 10 % $H_2/N_2$ at 350 $^o$C

prior to activity tests. A glass condenser at 0 $^o$C was used to separate liquid products

from gaseous products. The product gases, CO, $CO_2$, and $H_2$, were separated using MS-

5A and PPQ columns, and analyzed on-line by means of a MTI Quad Micro GC (Model

Q30L) equipped with a TCD.


*Selective CO Methanation Catalysts*

Selective CO methanation was conducted in a 4mm i.d. fixed-bed quartz tubular reactor

at ambient pressure. Two K-type thermal couple reactors were installed in the reactor in

such a way to measure the temperatures of the inlet and catalyst bed. 0.10g of catalyst

(60-100mesh particle size) was packed in the reactor. Unless otherwise noted, the

catalyst was reduced using a 10%$H_2/N_2$ gas mixture at 350 $^o$C for 2 hours prior to the run.

A pre-mixed gas containing 1%CO, 26%$CO_2$, and 73%$H_2$ (Matheson) was introduced

into the system using a Brooks Mass Flow Controller (5850E series). Water was fed into

a micro-channel vaporizer using a syringe pump (Cole Parmer 74900 series). The water

was vaporized at 200 $^o$C where it was mixed with the pre-mix gas and fed to the reactor.

The resulting feed mixture containing approximately 0.9%CO, 24.5%$CO_2$, 68.9%$H_2$, and

5.7%$H_2O$.  A moisture condenser and dry-rite bed were used to remove liquid materials

from the products.  The gaseous effluent was analyzed using a MTI GC (Model Q30L)

equipped with MS-5A and PPQ columns and a thermal conductivity detector (TCD).  For

measuring CO concentrations less than 1000 ppm, an infrared ZRH gas analyzer

(California Analytical Instruments) was used.  Unless otherwise noted temperature

profiles were collected maintaining a space velocity (SV) of 13,500 $hr^{-1}$.


## 2.3  Catalyst Characterizations

X-ray diffraction (XRD) patterns were collected on a Philips X'Pert MPD (Model

PW3040/00) diffractometer using Cu Kα radiation.  The diffraction patterns were

analyzed using Jade 6 (Materials Data Inc., Livermore, CA) and the Powder Diffraction

File database (International Centre for Diffraction Data, Newtown Square, PA.).  The

crystallite sizes were determined from the diffraction data using the Scherrer equation

and a Gaussian shape factor of 0.9.  All peaks above the background were profile-fitted

using Pearson VII models with an exponent of 1.5.  The full widths at half maximum

(FWHMs) were corrected for instrumental broadening, and the instrument function was

determined from a measurement of NIST SRM 640b (Silicon) under the study conditions.

The corrected FWHM's of all peaks were utilized in the Sherrer calculations, so the

reported crystallite sizes are independent of direction (*hkl*) and represent average values

in all cases.  BET measurement ($N_2$ adsorption/desorption) was obtained using an

Autosorb-1 (Quantachrome) apparatus.  BET measurement ($N_2$ adsorption/desorption)

was obtained using an Autosorb-1 (Quantachrome) apparatus.

Transmission electron microscopy imaging was conducted on a JEOL 2010 high-resolution analytical electron microscope operating at 200 kV with a $LaB_6$ filament. Powder samples were collected on copper grids with Formvar/carbon support film. High-resolution images were collected and analyzed by Gatan DigitalMicrograph® 3 software.

## 3. Results and Discussion – *Methanol Steam Reforming Catalysis*

### 3.1  PdZn Alloy Formation: Cause for Mechanism Change

XRD patterns for 16.7%Pd/ZnO catalysts are shown in Figure 1[9]. Spectra of fresh Pd/ZnO calcined at 350C showed diffraction peaks ascribed to ZnO only. No peaks were detected for Pd or PdO, suggesting the presence of PdO is below the detection limit of the XRD. After calcinations at 600C, a small PdO peak can be seen due to the sintering and formation of larger PdO particles. After calcination at $350^{o}C$ and evacuation at 600C the presence of metallic Pd can be detected at $2\theta$=40.1, and 46.6, due to the reduction of PdO via evacuation. Additional XRD patterns for the same catalyst were taken after reduction at $350^{o}C$ and being exposed to reaction conditions up to $300^{o}C$. It can be seen that metallic Pd is not detected but rather the presence of a PdZn alloy. As another comparison, the spectra of a sample after TPR reaction (reduction temperatures greater than $350^{o}C$ were used). Again, the formation of a PdZn alloy can be seen. This clear distinction between metallic palladium and the alloy makes XRD spectra a valuable tool in evaluating which phase is predominates. A PdZn alloy is formed under reduction conditions and at temperatures of at least $350^{o}C$. This is consistent with previous reports[8].
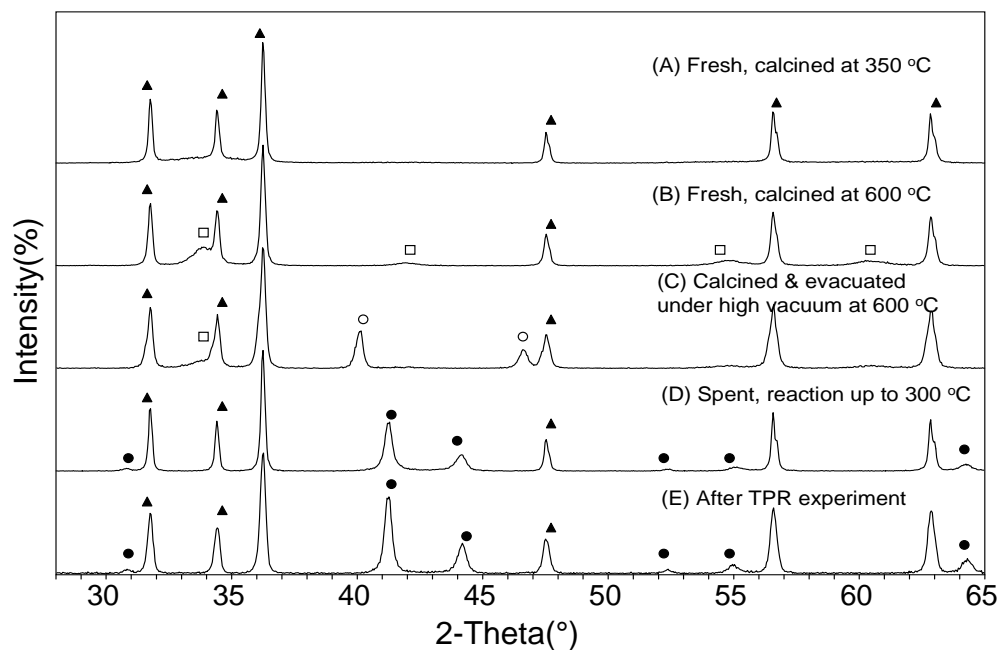
**Figure 1**. X-ray diffraction patterns of 16.7 wt% Pd/ZnO (a) fresh, calcined at 350 °C, (b) fresh, calcined at 600 °C, (c) calcined and evacuated under high vacuum at 600 °C, (d) spent, after reaction up to 300 °C, and (e) after TPR to 600 °C, showing diffraction peaks of ZnO (triangle), PdO (open square), Pd (open circle), and PdZn (filled circle). Reaction conditions: 0.1925g catalyst, 100 ms contact time or 36 000 GHSV, $H_2O/C = 1.8$, 1 atm. TPR conditions are the same as Figure 2[9].

The methanol conversion and CO selectivity over 4.8, 9.0, and 16.7% wt% Pd/ZnO catalysts are shown in Figure 2a and 2b, respectively. The activity data was obtained either after prior in situ reduction at 350°C or at 125°C. For the samples reduced at 350°C, an increase in conversion with increasing Pd loading can be observed. Complete methanol conversion is achieved as low as 300°C. The CO selectivity remained at of less than 5% for the entire temperature range examined. To compare the effect of reduction temperature, the 16.7% catalyst was reduced at a lower temperature of 125C (instead of 350°C) and tested under the same conditions. While the conversion for both the 350°C

reduced catalyst and the 125$^{o}$C reduced catalyst are approximately the same, the CO

selectivity is significantly higher.  At 280$^{o}$C, the CO selectivities are approximately 3%

and 13% for the catalysts reduced at 350$^{o}$C and 125$^{o}$C, respectively.  This can be

attributed to the PdZn alloy formation in the catalyst reduced at higher temperatures.  It

has been well established that Pd can be reduced at temperatures of at least 125C.  Thus,

upon reaction conditions, the metallic Pd catalyzes the methanol decomposition reaction

Eq (3), producing large amounts of CO before some of the CO is shifted to CO2 Eq(2).

But after PdZn alloy formation, upon reduction temperatures in excess of 350C, methanol

steam reaction Eq(1) predominates the methanol decomposition reaction Eq (3).  This

results in a selective reaction to CO2 and H2 with only small amounts of CO being

produced.
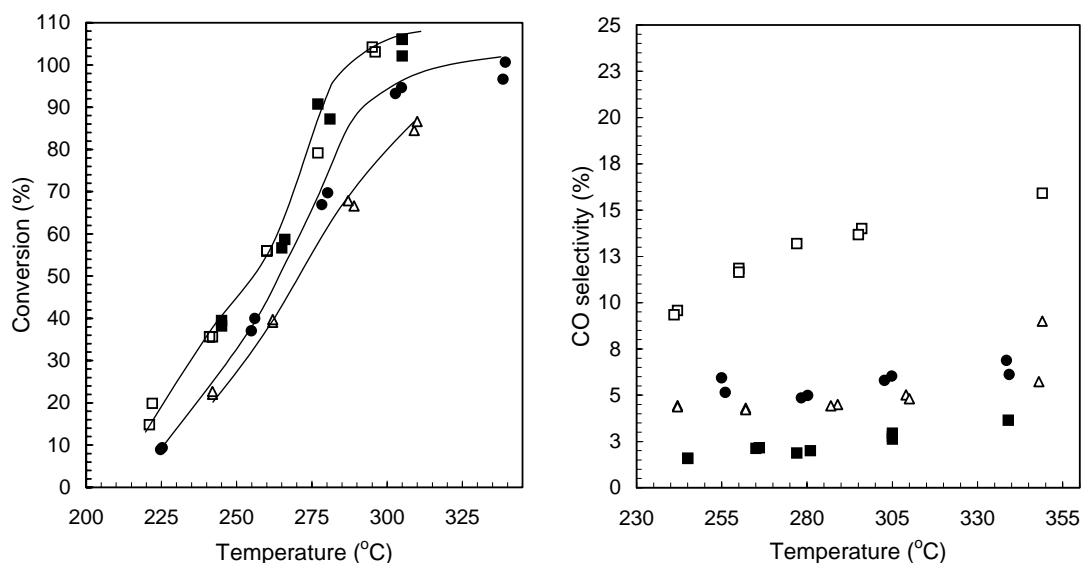
**Figure 2a and 2b.** Methanol conversion temperature profile under steam reforming of methanol (a) and the corresponded CO selectivity (b) for 4.8 wt% (triangle), 9.0 wt% (circle), and 16.7 wt% Pd on ZnO (both filled and open square). For 16.7%Pd/ZnO, the conversion profiles were acquired after two separate reduction temperatures: reduction at 125 °C (open square) and after reduction at 350 °C (filled square). All other catalysts were tested after reduction at 350 °C. Reaction conditions: 0.1925g catalyst, 100 ms contact time or 36000 GHSV, $H_2O/C = 1.8$ (molar), 1 atm.

## 3.2 Crystallite Size Effect

To further study the unique performance of the PdZn catalyst, a series of catalysts were prepared with increasing metal loadings of 0.5, 2.5, and 10%Pd, all on ZnO. This particular series was synthesized using an organic precursor since it been previously found that the impregnation of Pd using the highly acidic Pd nitrate aqueous precursor alters the textural properties such porosities and crystalline structures of ZnO,, where dissolution is evident[12]. Thus, an acetate precursor was used to avoid the complexities of

19

this phenomenon. These catalysts were reduced in situ at 425$^o$C prior to running the

reaction, thus facilitating the PdZn alloy formation. In Figure 3a, the activity

enhancement with increasing metal content can be seen. In Figure 3b, the CO selectivity

is shown. Interestingly, the lower Pd loadings exhibit the highest CO levels. The CO

selectivity for the 0.5% and 2.5%Pd level loadings decrease with temperature. While

excess Zn is present in all cases, it is intuitive to think that the possibility for increased

presence of metallic Pd would be more prevalent with the higher Pd loadings. As already

discussed, the existence of metallic Pd promotes decomposition, and hence, CO

formation. However, it is the lower Pd levels that produce more CO. Thus, as further

discussed later, it is hypothesized that crystallite size may play a keep role in determining

the reaction mechanism bias between steam reforming and decomposition.
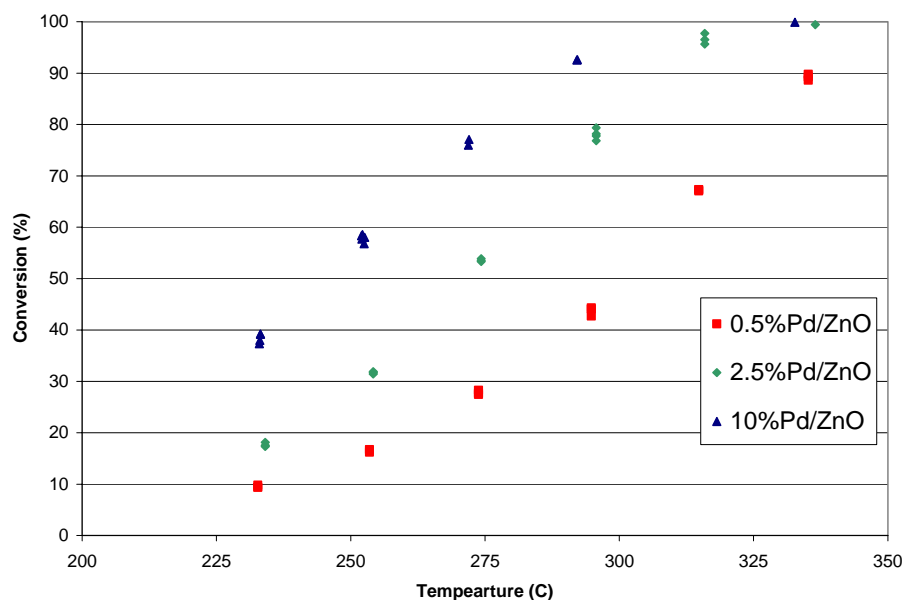


**Figure 3a:** Conversion as a function of reaction temperature for the organically
prepared series Pd/ZnO catalysts (GHSV=14,400 hr$^{-1}$, 1 atm, H$_2$O/C=1.8 (molar),
P$_{N2}$=0.25atm).
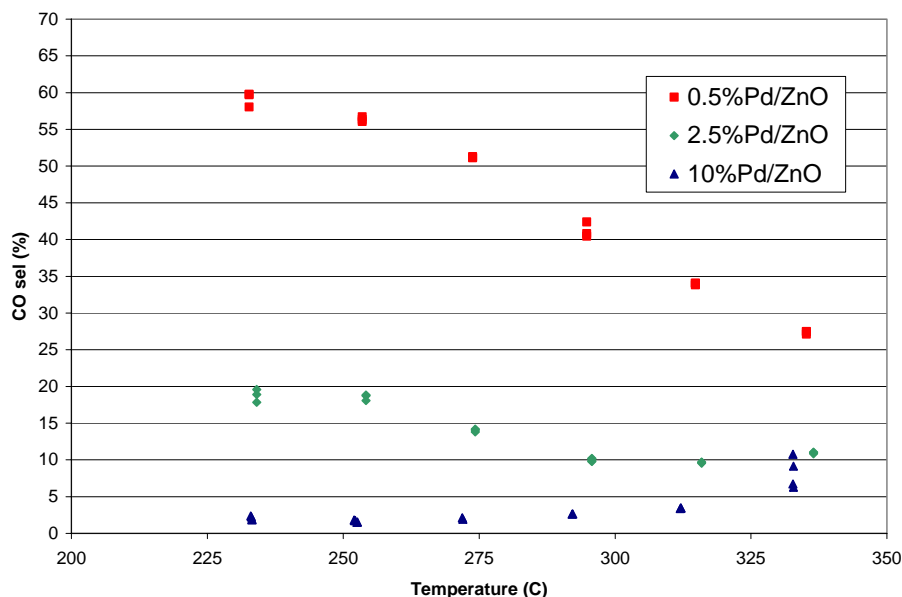
**Figure 3b:** CO selectivity as a function of reaction temperature for the organically prepared series Pd/ZnO catalysts (GHSV=14,400 hr$^{-1}$, 1 atm, H$_2$O/C=1.8 (molar), P$_{N2}$=0.25atm).

To study the effect of crystallite size on activity, this series of catalysts was reduced under increasing temperatures, then tested for activity at 275$^o$C, after each reduction temperature. In Figure 4a it can be seen that with increasing reduction temperature, the 10%Pd catalyst loses some conversion decreasing from 76% to 62% conversion at reduction temperatures of 350$^o$C and 650$^o$C, respectively. The 2.5%Pd catalyst loses some activity, with conversions from 52%, decreasing to 44% after reduction at 650C. The 0.5%Pd loading catalyst only slightly deactivated from 24% to 22%. For all three cases, the decrease in conversion is most likely due to the loss of active metal surface area due to metal sintering. While the higher 10%Pd loading deactivated the most, this is likely due to the fact there was more metal surface area to sinter. All three catalysts may have shown roughly similar reduction in activity on a percentage basis. In Figure 4b the

CO selectivity as a function of reduction is shown. As previously discussed, the CO selectivity is interestingly high even with the abundance of ZnO for the Pd to alloy, particularly for the lower 0.5%Pd loading. However, with increasing reduction temperature, the CO selectivity dramatically decreases for the 0.5%Pd loading catalyst. Increasing the reduction temperature from $350^{\circ}$C to $650^{\circ}$C decreases the CO selectivity from 49% to 18%. This greater than 60% decrease in CO selectivity, on a percentage basis, is far greater than the relatively slight decrease in conversion. There is little change in CO selectivity for the higher loading Pd catalysts; although there exists an initial decrease in CO selectivity when the 2.5%Pd and 10%Pd catalyst reduction temperatures are increased from $350^{\circ}$C to $425^{\circ}$C. Furthermore, there is a slight increase in CO selectivity for the 10%Pd loading catalyst when the reduction temperature is increased $500^{\circ}$C to $575^{\circ}$C. These findings suggest that PdZn crystallite size may play a role in the mechanism. With increased reduction temperature, the PdZn (and any metallic Pd) crystallites will increase in size. If it is assumed that PdZn is predominately present , as opposed to metallic Pd, perhaps there is a minimum crystallite size necessary to enhance the methanol reforming reaction Eq(1) over the methanol decomposition Eq(3) reaction.
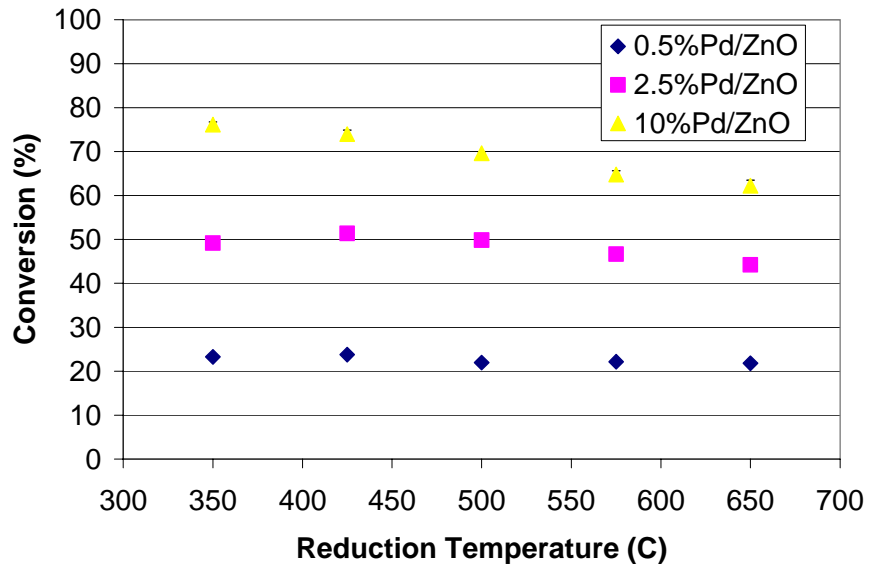
**Figure 4a:** Conversion as a function of reduction temperature for the organically prepared series Pd/ZnO catalysts (GHSV=14,400 hr$^{-1}$, 275$^{o}$C, 1 atm, H$_2$O/C=1.8 (molar), P$_{N2}$=0.25atm).
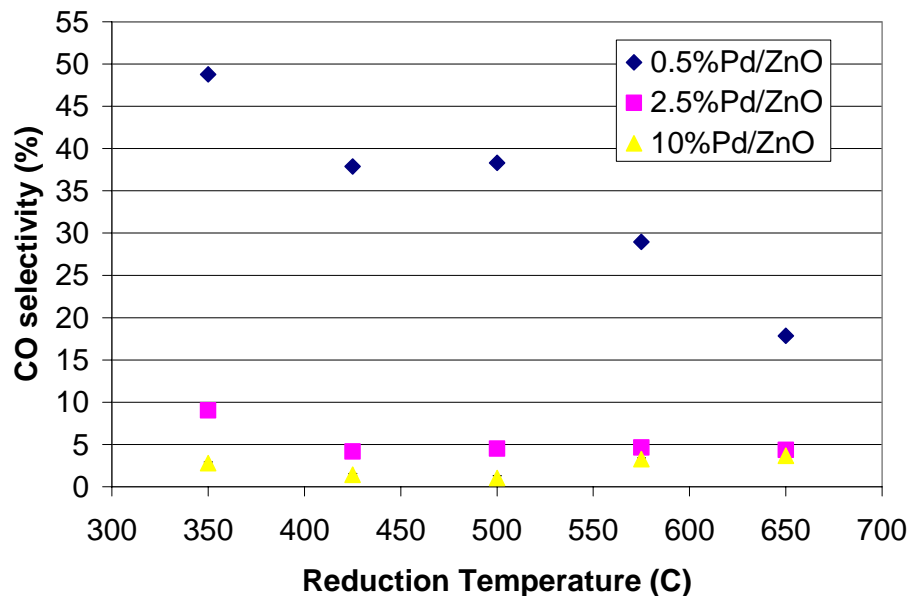
**Figure 4b:** CO selectivity as a function of reduction temperature for the organically prepared series Pd/ZnO catalysts (GHSV=14,400 hr$^{-1}$, 275$^{\text{o}}$C, 1 atm, H$_2$O/C=1.8 (molar), P$_{N2}$=0.25atm).

In an attempt to quantify this effect of increasing reduction temperature on CO selectivity, the crystallite sizes were studied for the catalysts reduced at 425$^{\text{o}}$C and also for those reduced at 600$^{\text{o}}$C. For the 0.5% and 2.5%Pd catalysts, supported on ZnO, due to the detection limits, no Pd or PdZn peaks were found in the XRD spectra – even for the 650$^{\text{o}}$C reduced catalysts (which would have the largest crystallite sizes due to sintering). Therefore, TEM was used to count crystallite sizes. Histograms of the crystallite size counts were done for the 0.5%,2.5%, and 10% catalysts after reductions at both 425$^{\text{o}}$C and 650$^{\text{o}}$C. The averages of these histograms were used to determine an average crystallite size. Figure 5a shows one TEM picture for the 10%Pd/ZnO catalyst; after reduction at 425$^{\text{o}}$C the average crystallite size was found to be 8.7nm. The other TEM pictures for this series are not shown. Not surprisingly, the crystallite sizes for each

24

metal loading increased with reduction temperature. For example, the crystallite for the

10%Pd/ZnO catalyst, after 650C reduction, increased to 11.4nm. This behavior was even

more pronounced for the other two catalysts. Figure 6 depicts the crystallite sizes found

at the two different reduction temperatures as a function of CO selectivity. The smaller

crystallite sizes exhibit high CO selectivities. The larger crystallite sizes have CO

selectivities less than 5%. While there are certainly limited data points, it appears there

could be a minimum CO selectivity after which increasing crystallite size favors slightly

more CO. However, more data points with larger crystallites would be necessary to make

this a clear distinction. Also, if the alloy was not completely formed with the lower metal

loadings, the presence of any metallic Pd would greatly affect these results (in which case

the Pd phase would be more a factor than the crystallite size). To prove the assumption

that the PdZn alloy is predominately present in the lower loading catalysts, one could

possibly use high resolution TEM. By imaging in on any particles found on the TEM

spectra, it is possible to examine the d-line spacing of the crystallites. The atomic

spacing of PdZn, Pd and PdO are uniquely different, with d-line spacings of 2.07, 2.25,

and 2.82A (+/-0.10A), resectively[4,9]. Other methods such as FTIR and TPD may also

gain useful insight in quantitatively determining the presence of metallic Pd
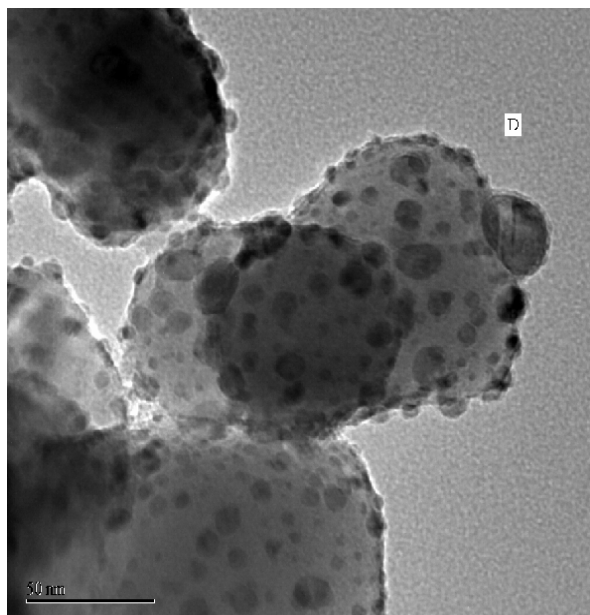
**Figure 5:** TEM micrograph on 10%Pd/ZnO after 425°C reduction for a) an organically prepared catalyst and b) using aqueous preparation.
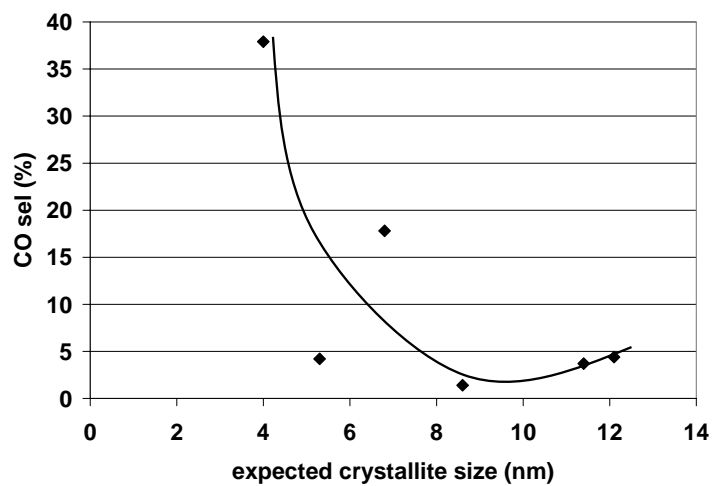


**Figure 6**: Expected crystallite size found from TEM as a function of CO selectivity (GHSV=14,400 hr$^{-1}$, 275°C, 1 atm, H2O/C=1.8 (molar), $P_{N2}$=0.25atm).

### 3.3 Pd/ZnO Supported on Alumina

To study the effects of surface area on methanol steam reforming and selectivity to CO, a series of alumina supported Pd/ZnO catalysts were investigated and compared to a non-supported Pd/ZnO catalyst and, for comparison purposes, a commercial CuZnAl catalyst. These catalysts were tested at a GHSV of 14,400 $hr^{-1}$ and steam/carbon =1.78.  The neutral alumina used for the Pd/ZnO supported catalysts had a surface area of $230 m^2/g$. The non-supported Pd/ZnO catalyst had a surface area of less than $10 m^2/g$.  In Table 1 below, a comparison of the three catalyst types is made.  The Pd loading, for this comparison was very similar – 8.6% and 8.9%Pd for the non-supported and supported catalysts, respectively.  The copper content of the commercial catalyst is not exactly known but from is expected to be on the order of 30wt%[17].  With alumina support the conversion is dramatically increased from 14.3% to 46.5%, under the same conditions using a gas-hour-space-velocity basis.  Likewise, the rate of hydrogen production, on a per-gram of catalyst basis, was increased from $1,616 cm^3/g/hr$ to $4,100 cm^3/g/hr$.  It can be seen that the conversion and hydrogen production of the supported catalyst was very similar to that of the commercial CuZnAl catalyst, which had a 46.3% conversion and $4,175 cm^3/g/hr$ hydrogen production.  All three cases had CO selectivities greater than 99%.  These results indicate the dramatic increase in activity by using a high surface area support.  Furthermore, by using a high surface area support, catalyst performance is comparable to that of a commercial CuZnAl catalyst, which had not before been reported. Although Pd/ZnO catalysts have many advantages over Cu based catalysts, PdZnO have been previously reported to be less active than Cu based catalysts[4].

**Table 1**. Summary of steam reforming activity comparisons at 220ºC (GHSV = 14,400 hr$^{-1}$, Steam/carbon =1.78)[4].

| Component | Pd/ZnO Baseline | Pd-ZnO/Al$_2$O$_3$ | CuZnAl Sud-Chemie |
|---|---|---|---|
| Pd loading, wt% | 8.6 | 8.9 | - |
| Conversion, % | 14.3 | 46.5 | 46.3 |
| CO$_2$ Selectivity, % | 99.2 | 99.4 | 99.8 |
| r$_{H2}$ (cm$^3$/g/h) | 1,616 | 4,100 | 4,175 |

To study the effect of Pd:Zn ratio on methanol steam reforming and CO selectivity, a series of catalysts with varying Pd:Zn ratios and Pd loadings was also investigated[4]. Table 2 summarizes the metal contents of these catalysts and temperatures required to reach 80% methanol conversion, CO selectivity, and hydrogen production[4]. Comparing the catalysts with increasing Pd:Zn ratio, the conversion increases with increasing Pd:Zn ratios from 0.08 to 0.38, corresponding with a slight decrease in CO selectivity. Increasing Pd:Zn ratio corresponds to increasing CO selectivity and decreasing activity for ratios larger than 0.38. This trend is depicted in Figure 7, for the activity results at a temperature of 260ºC[4]. From XRD patterns, for the catalysts with varying Pd:Zn ratios, it was observed that metallic Pd was present, as well as PdZn alloy, in the catalysts containing Pd:Zn ratios higher than 0.38[4]. Due to the XRD detection limits, no Pd or PdZn phase was detected for the catalysts with Pd:Zn ratios of 0.38 and less. By using high resolution TEM, only the distinct d-lines for that of the PdZn alloy was found for the PdZnAl-38A catalyst, with Pd:Zn ratio of 0.38. On the contrary, d-lines for metallic Pd was found in the PdZnAl-110 catalyst, which had a Pd:Zn ratio of 1.10[4]. Thus, it is hypothesized that the increasing CO selectivity, observed for the catalysts of increasing

28

Pd:Zn ratios higher than 0.38, is due to the increasing presence of metallic Pd. This is

likely due to the increasing enhancement of the methanol decomposition reaction, which

predominantly occurs over metallic Pd surfaces. As the metallic Pd levels rise, so to does

the selectivity of the methanol decomposition reaction Eq(3).

**Table 2**. Summary of catalysts and methanol steam reforming activities (GHSV = 14,400 hr$^{-1}$, Steam/carbon =1.78)[4].

| Sample ID | Pd (wt%) | Pd:Zn (mol/mol) | 80% conversion of methanol | | |
|---|---|---|---|---|---|
| | | | Temp. ($^{o}$C) | Selectivity to CO (%) | Rate of H$_2$ (mol/g-Pd•hr) |
| PdZn, baseline | 8.6 | 0.09 | 297 | 2.3 | 4.2 |
| PdZnAl-8 | 2.6 | 0.08 | 275 | 2.2 | 13.1 |
| PdZnAl-17 | 5.0 | 0.17 | 265 | 1.7 | 8.2 |
| PdZnAl-38A | 8.9 | 0.38 | 250 | 1.4 | 4.1 |
| PdZnAl-76 | 12.9 | 0.76 | 282 | 8.7 | 3.0 |
| PdZnAl-110 | 15.7 | 1.10 | 285 | 23.5 | 2.2 |
| PdZnAl-38B | 6 | 0.38 | 265 | 3 | 6 |
| PdZnAl-38C | 4.5 | 0.38 | 273 | 5 | 8.1 |
| PdZnAl-38D | 3 | 0.38 | 283 | 7 | 12 |
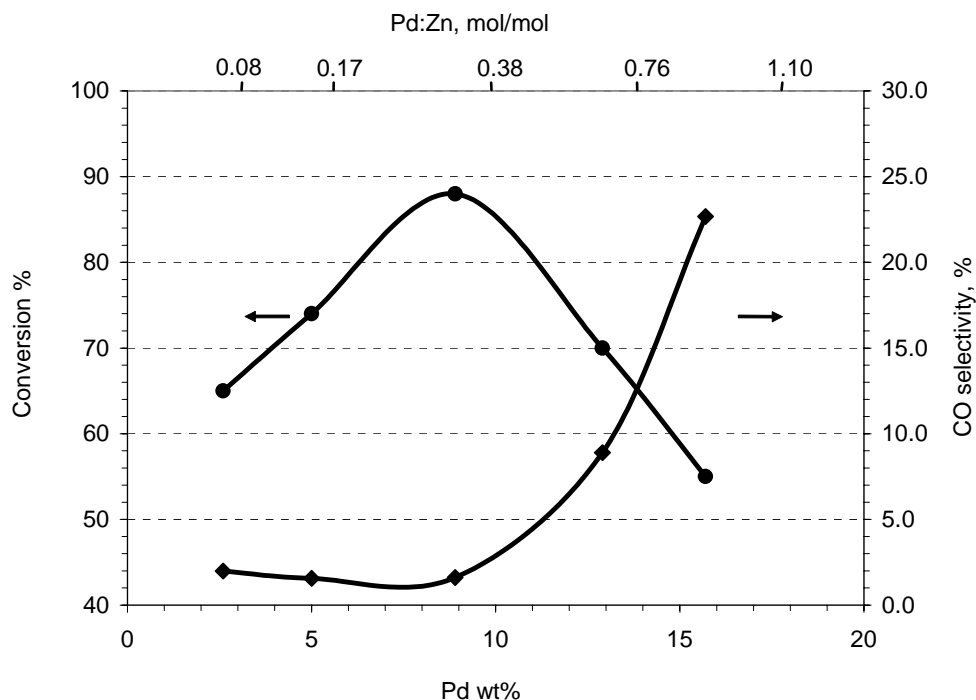
**Figure 7.** Methanol conversion and CO selectivity as functions of Pd/Zn ratio and Pd loading (260°C, GHSV = 14,400 hr^{-1}, Steam/carbon =1.78)[4].

To study the effect of Pd level, while maintaining the optimum Pd:Zn ratio of 0.38 found in the previous section, a series of catlasyts were investigated containing 3%, 4.5%, 6% and the one previously mentioned containing 8.9%Pd[4]. The catalyst content and activity summary is also included in Table 2. Not surprisingly, with increasing Pd content the conversion also increased. However, increasing Pd content also decreased CO selectivity, even while maintaining a constant Pd:Zn ratio of 0.38. It should be noted that there is also a temperature increase for the CO selectivities reported in Table 2, with increasing Pd loadings. This is since the values were reported for the CO selectivities at which 80% methanol conversion was observed, and the lower Pd loadings required higher temperatures. However, this phenomena is also observed when the same temperatures are considered. The activity results at a temperature of 270°C, for the

catalysts with increasing Pd content and Pd:Zn ratio of 0.38, is depicted at a temperature

Table 3. The CO selectivities increase from 1.5, 3.0, 4.8, and 6.4% for the catalysts with

8.9, 6.0, 4.5 and 3.0%Pd metal loadings, respectively. While the Pd:Zn remains constant,

there is a decrease in CO selectivity with increasing Pd content. It was previously

thought that there could only be more metallic Pd with higher metal loading, if any

significant phase difference.

**Table 3**. Isothermal activity comparison of catalysts with Pd:Zn=0.38 (GHSV = 14,400 hr$^{-1}$, 270$^{o}$C, Steam/carbon =1.78)[4].

| Sample ID | Pd (wt%) | Pd:Zn (mol/mol) | Temperature=270$^{o}$C | |
|---|---|---|---|---|
| | | | Selectivity to CO (%) | Methanol Conversion (%) |
| PdZnAl-38A | 8.9 | 0.38 | 1.5 | 90 |
| PdZnAl-38B | 6 | 0.38 | 3.0 | 82 |
| PdZnAl-38C | 4.5 | 0.38 | 4.8 | 75 |
| PdZnAl-38D | 3 | 0.38 | 6.4 | 65 |

To explain the difference in CO selectivity, it is hypothesized that there are two possible

explanations. Either there could be a differentiation in the type of alloy being formed

with different Pd contents, or there could be a crystallite size effect. If is possible that if

the different PdZn alloys formed had varying degrees of Pd or Zn present, there would be

a difference in activity. In this case, the Pd:Zn ratio remained constant. Thus, at this

point, it seems more likely that the crystallite size may play a role. It was previously

discussed in section 3.2 that with increasing Pd loading, there was a corresponding

increase in crystallite size. It is very likely that this is also occurring in this case as well.

Thus, it is possible that a large enough crystallite size is needed to enhance the methanol

reforming reaction Eq(1) while minimizing decomposition Eq(3) and/or the water-gas-

shift reaction Eq(2). The decomposition and/or water-gas shift may be favored with lower crystallite sizes. Further studies could be made to study the effects of crystallite size. Specifically, to elucidate crystallite size effects between reforming Eq(1), water-gas-shift Eq(2), and decomposition Eq(2) reactions.

## 3.4  Steam-to-Carbon Ratio & Kinetics

To study the effect of steam-carbon ratio, a 10%Pd/ZnO/Al$_2$O$_3$ catalyst was tested using steam to carbon ratios, on a molar basis, of H$_2$O/C=1.0, 1.2, 1.5, and 1.8. The runs for all four steam-to-carbon ratios had approximately the same conversion. At 320$^o$C, the methanol conversion was approximately 80%, under the conditions tested. In Figure 8, it can be seen that at a temperature of 320$^o$C, the CO selectivity for the ratios of 1.2, 1.5, and 1.8 were all very similar, between 2.5% and 3.0%. For H$_2$O/C=1.0 , the CO selectivity increased to 4.8%. This is due to the fact that CO is thermodynamically favored at lower temperatures. Nonetheless, for all the steam to carbon ratios investigated, the CO selectivities remain well below equilibrium levels (as depicted in Figure 8). For example, for a steam to carbon ratio of 1.2, the equilibrium CO selectivity is 18%, far greater than the 2.8% CO selectivity experimentally found. This finding is important for practical applications. Since this catalyst exhibits excellent selectivities at steam/carbon ratios approaching stoichiometery (H$_2$O/C=1 is required for steam reforming Eq(1)), there is not much need for excess water in the fuel mixture which might otherwise be necessary to lower the CO output (if a feed contained a steam/carbon ratio of 1 there would be no excess fuel if complete conversion were obtained). For example, a 5% CO selectivity can be achieved using this PdZn catalyst using a steam to carbon ratio of 1. If the CO were present under equilibrium levels, a 5% CO selectivity

would require a steam to carbon ratio in excess of 2. Thus, twice as much water would be needed. By decreasing the mixture fuel weight, helps to increase the energy density of a fuel processor system, which is extremely important for portable power applications.
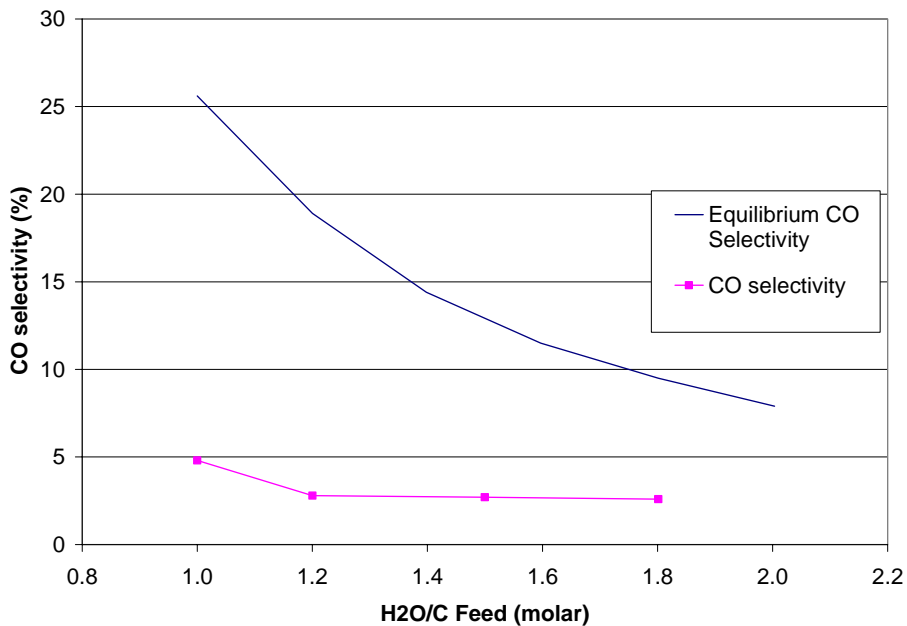


**Figure 8:** CO selectivity as a function of feed steam/carbon ratio on 10%PdZnO/Al$_2$O$_3$ catalyst (GHSV=2100 hr$^{-1}$, 1 atm, 320$^o$C, methanol feed=0.27atm, water feed varied with N2 dilutent added to maintain constant GHSV for all runs).

By similar kinetic arguments, the benefits of increased throughput by increased reaction temperature without sacrificing much additional CO production can be seen. In Figure 9, CO selectivity as a function of temperature is shown, for the same 10%Pd/ZnO/Al$_2$O$_3$ catalyst depicted in Figure 7, under a steam to carbon of 1.2. Again, the CO levels are well below equilibrium. At 300$^o$C, the CO selectivity is approximately 2.5% (an approximate CO level of 1%). To achieve the same CO output under equilibrium

limitations would require a temperature of about $180^{\circ}C$. The result is a $120^{\circ}C$ operating temperature for the same CO concentration, resulting in a 200-fold increase in reaction rate, according to a previous kinetic study done at PNNL[2,12]. Thus, the kinetic advantages of the PdZnAl catalyst, compared to the CuZnAl catalyst, can also be described in terms of enhanced conversion rates. The CuZnAl catalyst cannot be operated at such high temperatures ($>280^{\circ}C$) due to stability issues. Furthermore, it has been shown in this study that a PdZnAl catalyst has demonstrated similar performance to that of a commercial CuZnAl catalyst, under identical, low temperature conditions ($220^{\circ}C$, Table 1). This makes the enhanced kinetics possible, by operating at temperatures $>280^{\circ}C$, a real advantage unique to the PdZnAl catalyst. Under such high temperature operation, increased throughputs can be achieved given the same amount of catalyst, when compared to the CuZnAl catalyst. According the same previous kinetic study mentioned above, increasing the temperature from just $280^{0}C$ to $310^{0}C$ increases the reaction rate almost 3-fold[12].
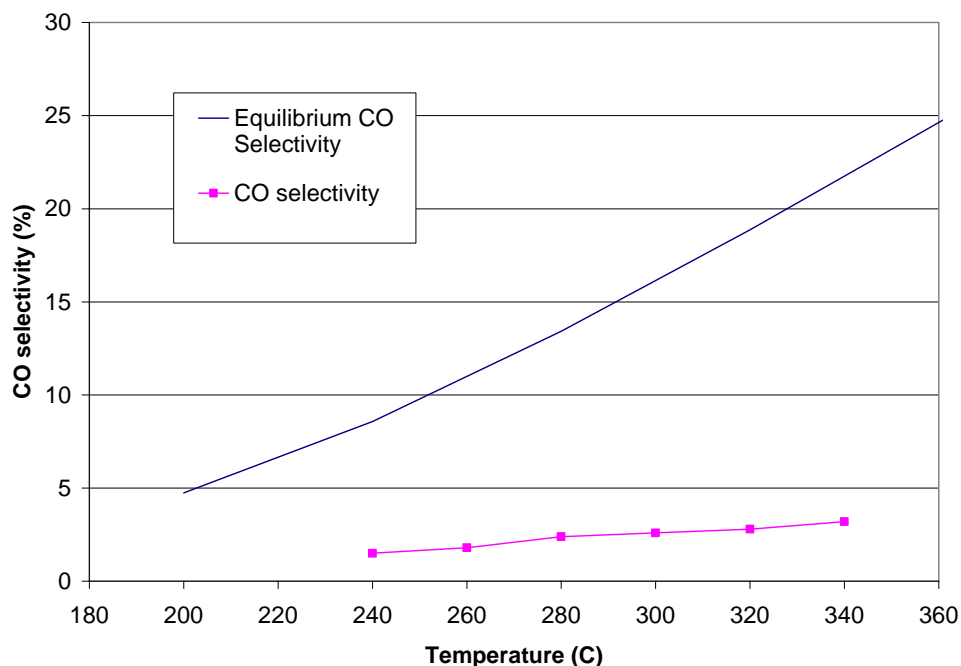
**Figure 9:** CO selectivity as a function of temperature on 10%Pd/ZnO/Al$_2$O$_3$ catalyst (GHSV=2100 hr$^{-1}$, 1 atm, H2O/C=1.2, P$_{N2}$=0.4 atm).

## 4. Results and Discussion – *Selective CO Methanation Catalysis*

### 4.1 Catalyst Characterizations

A summary of the catalyst prepared, including the crystallite sizes, as determined from XRD data, and BET results are shown in Table 4. As a general trend, the crystallite sizes increase with increasing Ru loading, as expected. When comparing catalysts prepared with the same metal loading, the crystallite sizes increase with higher reduction temperatures and with more impregnations necessary to achieve the same metal loading For example, when comparing the single and multiple impregnated 5%Ru/Al$_2$O$_3$ catalysts, the average crystallite size increases from 9.1 to 14.4 nm, respectively. As might be expected, with sequential impregnations, a layering effect would occur resulting in ruthenium being deposited on top of previous ruthenium additions. With a single

impregnation, as with 5s-350, the active metal is more dispersed than with sequential

loadings, as with 5m-350.  Surface area measurements (BET) indicate that the catalysts

prepared on the alumina support have high surface areas of approximately 233 $m^2$/g,

while the $ZrO_2$ and $TiO_2$ supported catalysts have much lower surface areas of

approximately 60 and 9 $m^2$/g, respectively.  Crystallize sizes cannot be determined from

XRD spectrum for the $ZrO_2$ and $TiO_2$ supported catalysts due to metal and support peak

overlap.

**Table 4**:  Summary of Catalysts Prepared for Selective CO Methanation including XRD
crystallite sizes and BET surface areas.

| Catalyst ID[a] | Ru Amount (wt.%) | Support material | # Metal Solution Impregnations | Reduction Temperature ($^o$C) | Crystallite Size, XRD (nm) | BET Surface Area ($m^2$/g) |
|---|---|---|---|---|---|---|
| 1s-350 | 1 | $Al_2O_3$ | 1 | 350 | 3.8 | |
| 3s-350 | 3 | $Al_2O_3$ | 1 | 350 | 10.8 | 235 |
| 3s-600 | 3 | $Al_2O_3$ | 1 | 600 | 13.7 | |
| 3s-000[b] | 3 | $Al_2O_3$ | 1 | None | - | |
| 3m-350 | 3 | $Al_2O_3$ | 3 | 350 | 9.6 | 233 |
| 5s-350 | 5 | $Al_2O_3$ | 1 | 350 | 9.1 | |
| 5m-350 | 5 | $Al_2O_3$ | 5 | 350 | 14.4 | |
| 7s-350 | 7 | $Al_2O_3$ | 1 | 350 | 11.1 | |
| 3-ZrO2 | 3 | $ZrO_2$ | 6 | 350 | n/a | 69 |
| 3-TiO2 | 3 | $TiO_2$ | 6 | 350 | n/a | 9 |

[a]The first number used for the catalyst identification nomenclature is the ruthenium
percentage.  The "s" and "m" signify single and multiple impregnations, respectively.
The latter number represents the reduction temperature.  Thus, "1s-350" represents a
1%Ru/$Al_2O_3$ catalyst, done with a single incipient-wetness ruthenium solution
impregnation, reduced at 350 $^o$C.
[b]The 3s-000 catalyst was prepared via a single-step impregnation without any reduction
pre-treatment.

## 4.2  The Effects of Ru Loading

To study the effects of Ru loading on catalyst performance, a series of single impregnated catalysts were studied.  In Figure 10a it can be seen all catalysts except 1s-350 exhibit a rapid decrease in CO, usually within  20-30 $^{o}$C, reach a minimum CO level, then slowly increase CO content with temperature.  This is consistent with previous reports reporting rise in conversion with increasing metal loading[11,12,15].  The CO first begins to methanate, described by Eq (1).  Then, when the CO level is much reduced, $CO_2$ methanation, Eq (2), and the reverse shift reactions, Eq (3), take place.  The reverse shift reaction occurring is indicated by the slow increase in CO level.  As described in the introduction, according the Rehmat, et. al., it is shown that in the absence in $CO_2$, the CO methanation would go to completion.  However, we can see that, with $CO_2$ in the feed, the reverse shift reaction becomes more prominent as the temperature increases, thus, increasing CO content.  This results in a temperature window in which the CO output will be low enough for applicable use (typically somewhere <100 ppm) before CO levels rise to a level out of a useful range.  In Figure 10b it can be seen that the hydrogen consumption increases more rapidly once the majority of the CO is hydrogenated.  At this point, $CO_2$ methanation, Eq (2) begins to take place.  With increasing temperature hydrogen consumption continues to increase.
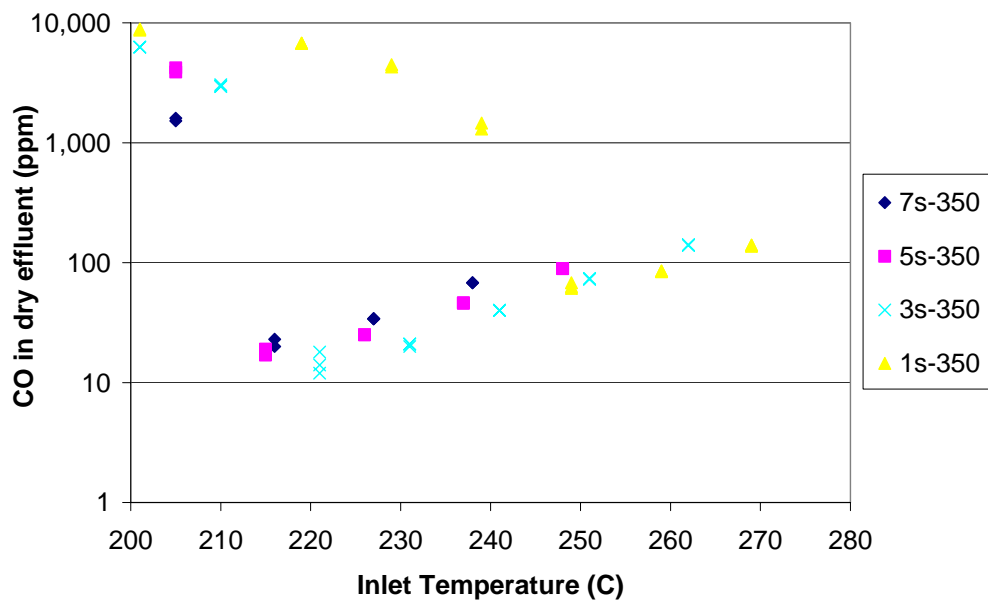
(A)
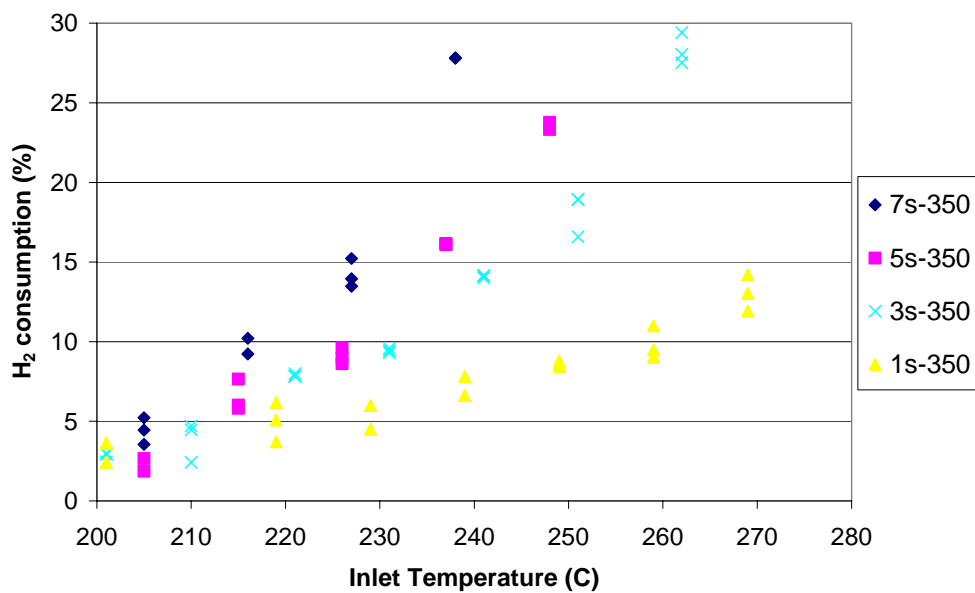


(B)

**Figure 10**:  Effect of Ru metal loading and temperature on a) CO concentration in the effluent and b) $H_2$ consumption (approximate feed composition:  0.9%CO, 24.5%$CO_2$, 68.9%$H_2$, 5.7%$H_2O$, SV=13,500 $hr^{-1}$).

The extent of CO output and hydrogen consumption with temperature is largely affected by Ru loading. The CO methanation activity, depicted in Figure10a, generally increases with metal loading. The 1% loading barely reaches a CO level of 100 ppm, at 250 $^{\circ}$C, before CO levels begin to increase. The other three catalysts are considerably more active reaching a much lower CO level between 10-20 ppm, at temperatures between 215 $^{\circ}$C and 220 $^{\circ}$C. The 3% loading catalyst has a slightly less active CO output profile than the 7% and 5% loading catalysts, which have similar profiles. This suggests that there is a maximum metal loading where any further increase fails to enhance CO methanation performance. However, the hydrogen consumption profiles show dramatic differences between all four catalysts. With increasing metal loading, hydrogen consumption increases. $CO_2$ methanation more quickly occurs with increasing metal loadings. This is not surprising since it has been established that methanation for both $CO_2$ and CO will be enhanced as the number of active sites increase[15]. Thus, a balance of activity and selectivity must occur, with a large a temperature window as possible for optimum performance. A catalyst must be chosen to be active enough but not overly active where $CO_2$ methanation quickly dominates. In this case, the 3s-350 catalyst has almost the same CO output of the higher loading catalysts and exhibits far superior selectivity to the minimization of $CO_2$ methanation (and thus, hydrogen consumption).

**4.3  The Effects of Preparation and Pretreatment**

It was found that the catalyst performance is greatly affected by the impregnation method. In Figure 11a it is shown that when comparing catalysts with single and multiple impregnations, the catalyst with the single dispersion is more active for CO

removal.  Catalyst 3m-350 has a CO profile shifted to the right.  This also corresponds to a subsequent increase in $CO_2$ methanation.  Figure 11b shows the hydrogen consumption increasing substantially more quickly for the single impregnated catalyst.   This is attributed to the fact that the single-step impregnation method yields a better dispersed catalyst and thus, contains more active sites accelerating not only the CO, but also $CO_2$, methanation.  This phenomena is also observed for the 5% Ru loading catalyst, as depicted in Figure 12a and 12b.  The single step impregnated catalyst has a more active CO profile, shifted to the left.  However, it also methanates $CO_2$, and thus consumes hydrogen, more readily.  From Table 4, it can be seen  that the crystallite sizes for the 5s-350, and 5m-350 catalysts are 9.1 and 14.4nm, respectively, thus, indicating the dispersion differences.  It should be noted that there was no detectable crystallite size differences between the 3s-350 and 3m-350 catalyst from the XRD spectrum.  However, additional H2 chemisorption experiments performed on these two catalysts suggests that there is indeed an increase in dispersion with the single step, when compared to the multi-step catalyst, as would be expected.  It is thought that while the XRD profile fitting may suggest general, average crystallite size trends, it is not completely accurate and only represents approximate ranges.
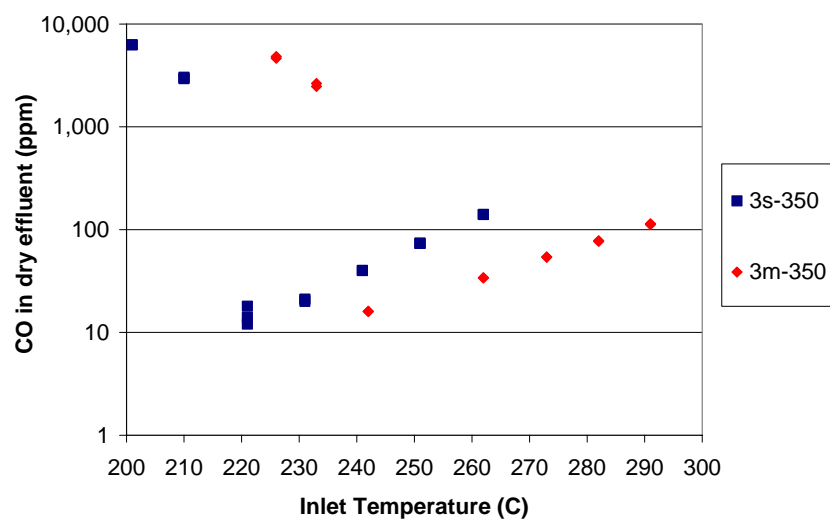
(A)
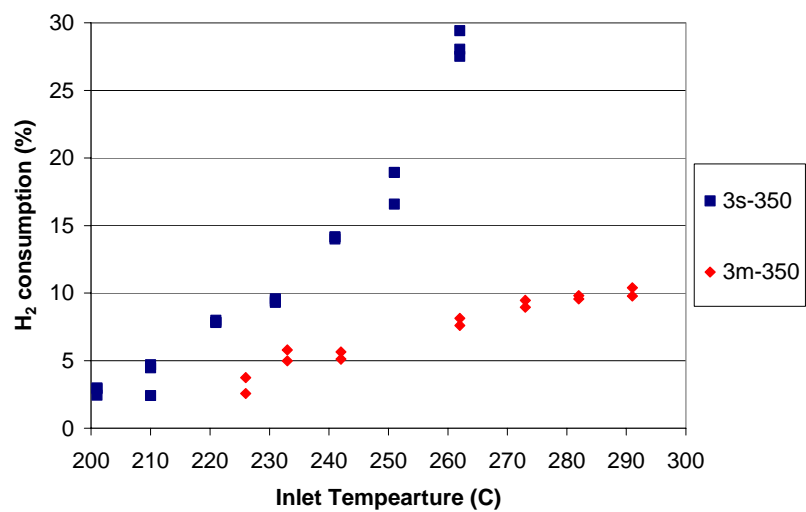


(B)

**Figure 11**: Effect of preparation and temperature, for a 3%Ru metal loading catalyst, on a) CO concentration in the effluent and b) $H_2$ consumption (approximate feed composition: 0.9%CO, 24.5%$CO_2$, 68.9%$H_2$, 5.7%$H_2O$, SV=13,500 hr$^{-1}$).
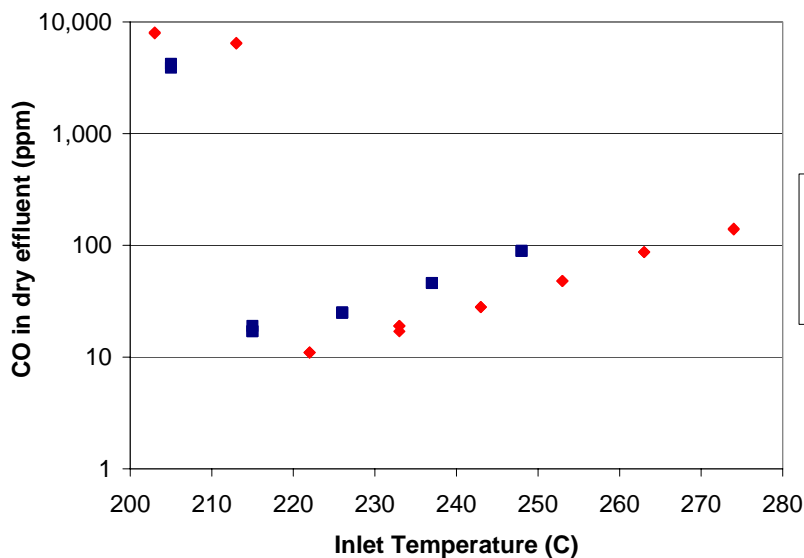
(A)
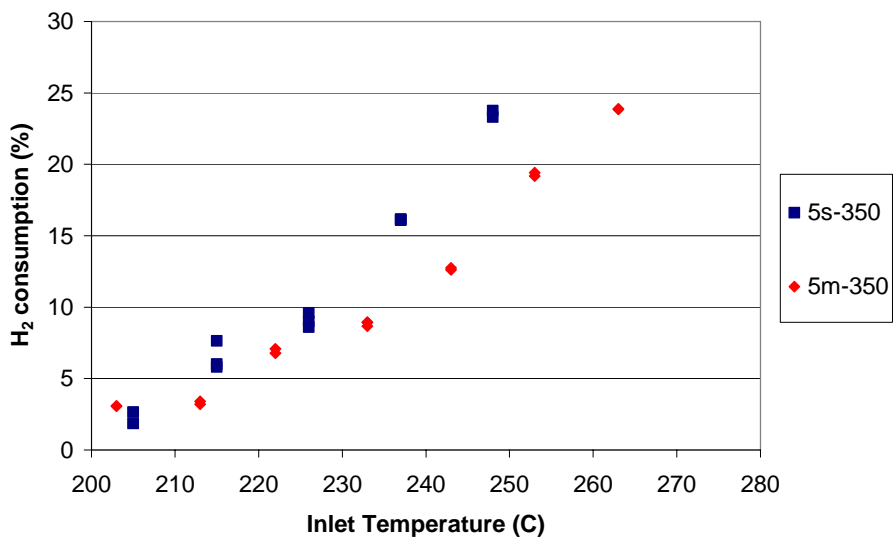


(B)

**Figure 12**:  Effect of preparation and temperature, for a 5%Ru metal loading catalyst, on a) CO concentration in the effluent and b) $H_2$ consumption (approximate feed composition:  0.9%CO, 24.5%$CO_2$, 68.9%$H_2$, 5.7%$H_2O$, SV=13,500 $hr^{-1}$).

While the more dispersed catalysts have initially more activity, the temperature window

comparisons between the two impregnation types have approximately the same CO level

range. For example, catalyst 3s-350 has a temperature range between approximately 220 $^{o}$C and 260 $^{o}$C where the CO level is less than 100 ppm. Catalyst 3m-350 has a window between 240 $^{o}$C and 280 $^{o}$C where it the CO remains below 100 ppm. It is believed that the CO level rises more quickly for the 3s-350 catalyst because $CO_2$ methanation is occurring more rapidly, thus also facilitating the reverse shift functionality. Thus, while the better dispersed catalysts are initially more active, the temperature windows for a given CO level are approximately the same when compared to the worse dispersed counterparts. Furthermore, the significant differences in selectivity suggest the larger crystallite sizes provide a more optimum range of operation. The 3m-350 catalyst consumes no more than 10% of the hydrogen, along the range studied.

The reduction temperature was also found to have a similar effect on performance. A 3% loading was tested with no reduction, and reduction at 350 $^{o}$C and 600 $^{o}$C (3s-000,3s-350, and 3s-600, respectively), shown in Figure 13A. Activity was similar between the catalysts without reduction and 350 $^{o}$C reduction. It is thought that while the first catalyst did not undergo a pretreatment reduction, the metal is quickly reduced to metallic Ru since the feed contains approximately 70% hydrogen. Thus, the ruthenium will sinter at the reaction temperature. Since the operating range never exceeds 300 $^{o}$C, the crystallite size under operating conditions should be smaller, than 3s-350 reduced at 350 $^{o}$C. Catalyst 3s-600 has a shift in the CO profile to the right. Correspondingly, the hydrogen consumption decreases with increasing reduction temperature, as shown in Figure 13b. These findings further indicate performance changes according to crystallite sizes, as seen when comparing catalysts with varying impregnation schemes, as described above.
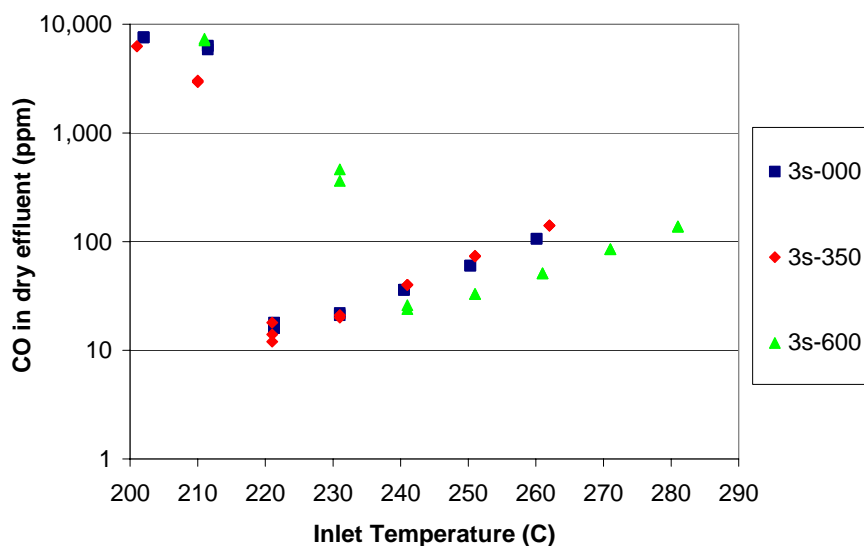
(A)
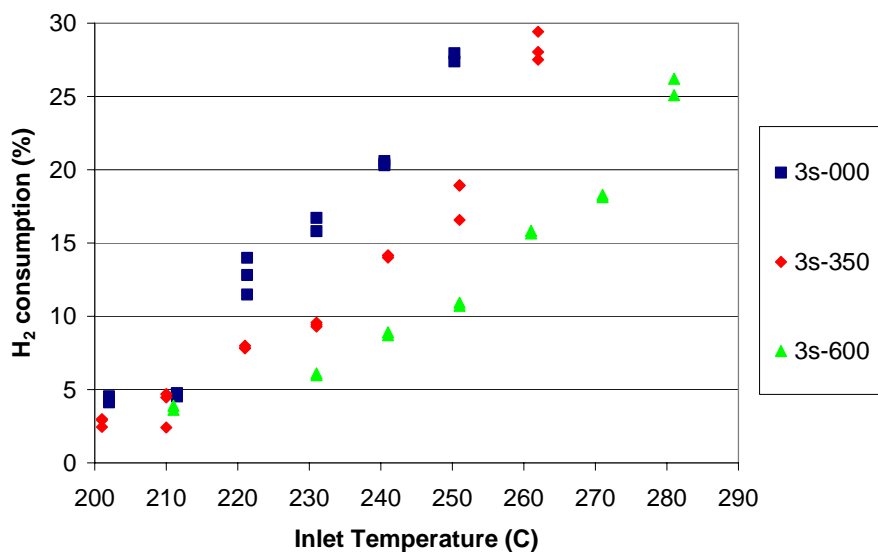


(B)

**Figure 13**: Effect of reduction temperature and operating temperature, for a 3%Ru metal loading catalyst, on a) CO concentration in the effluent and b) $H_2$ consumption (approximate feed composition: 0.9%CO, 24.5%$CO_2$, 68.9%$H_2$, 5.7%$H_2O$, SV=13,500 hr$^{-1}$).

## 4.4 The Effect of Support

To investigate the effect of support on performance, $ZrO_2$ and $TiO_2$ supported catalysts were studied. From Figure 14a it is seen that the activity of the $Al_2O_3$ far exceeds that of the other supports. The minimum CO level for the 3-$ZrO_2$ and 3-$TiO_2$ catalysts was 3080 ppm, and 636 ppm, respectively. Furthermore, the hydrogen consumption quickly accelerates for these catalysts once a minimum CO level is attained, as shown in Figure 14b. This can be attributed to the fact that the surface areas are much less; 69 and 9 $m^2$/g for the zirconia and titania supports, respectively (found in Table 1). Lower surface area catalysts yield more poorly dispersed catalysts. The $Al_2O_3$ catalyst with a higher surface area of 233 $m^2$/g, and better dispersion, enables CO methanation to occur quicker, at lower temperatures, and more selectively, before $CO_2$ methanation predominates at higher temperatures. The activity increases with surface area in the order of $Al_2O_3$ > $ZrO_2$ > $TiO_2$. Again, this is consistent with others who have argued CO methanation occurs more rapidly with increasing number of active sites[15].
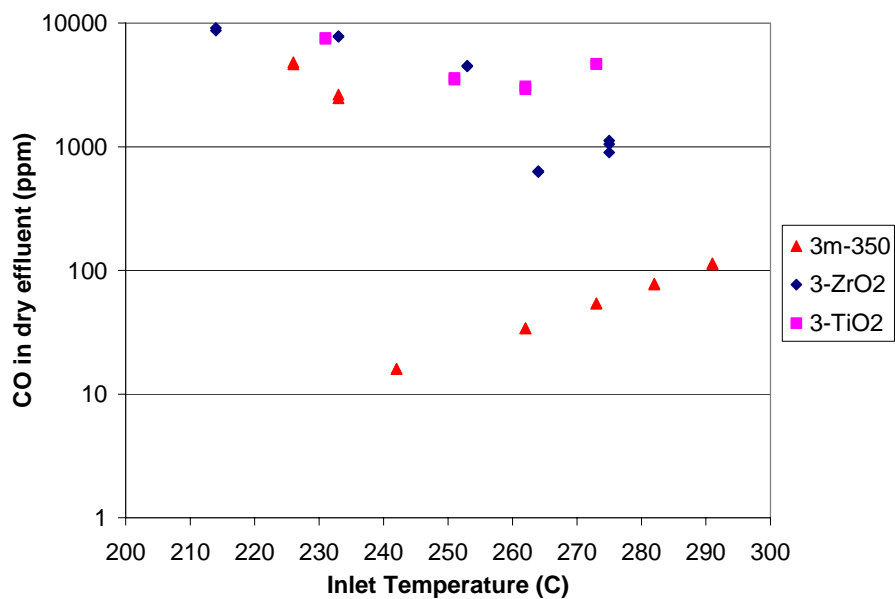
(A)
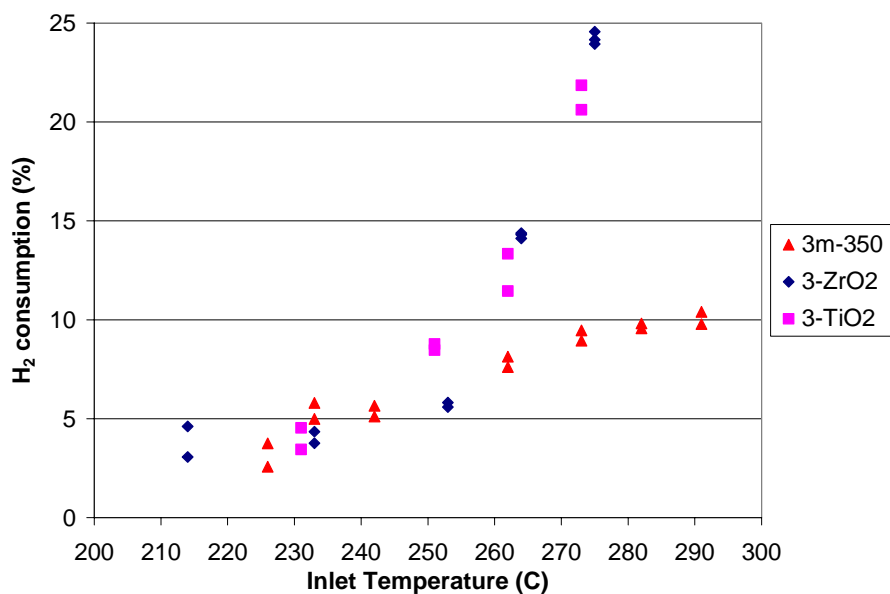


(B)

**Figure 14**: Effect of support for 3% loading and temperature on a) CO concentration in the effluent and b) $H_2$ consumption (approximate feed composition: 0.9%CO, 24.5%$CO_2$, 68.9%$H_2$, 5.7%$H_2O$, SV=13,500 $hr^{-1}$).

## 4.5 Stability under Oxidizing Conditions

From Figure 13a it has already been shown that catalyst 3s-000 is relatively active without any pretreatment, although the catalyst could be improved with optimizing reduction temperature. For portable fuel cell operations, catalysts may unavoidable be exposed to air, even at reaction temperatures. Catalyst stability in air is highly desired which help simplify the start up and shut down procedures. To evaluate the catalyst durability, the catalyst was exposed to air at reaction temperature ($260\,^{\circ}C$) for one hour, shutting down to room temperature under air, then starting up the next day after having left the catalyst flowing under air. From Figure 15a it can be seen that the catalyst performance was not noticeably affected. In fact, the catalyst selectivity was enhanced, as shown in Figure 15b. After having run under operating conditions up to $300\,^{\circ}C$, the 3s-000 catalyst had selectivities comparable to the 3s-350 catalyst, even after being exposed to air at reaction temperatures. One plausible explanation could be that oxidized ruthenium, $RuO_2$, could be the more active phase, as has recently been suggested with the case for CO oxidation reactions[25]. However, in this case, this notion is yet inconclusive since the reduced catalyst was treated at a higher temperature, and hence, the crystallite sizes are assuredly different. The possibility of crystallite size effect could mask any changes in selectivity due to a Ru oxidation state effect. As seen in the previous section, crystallite size plays a key role in catalyst performance.
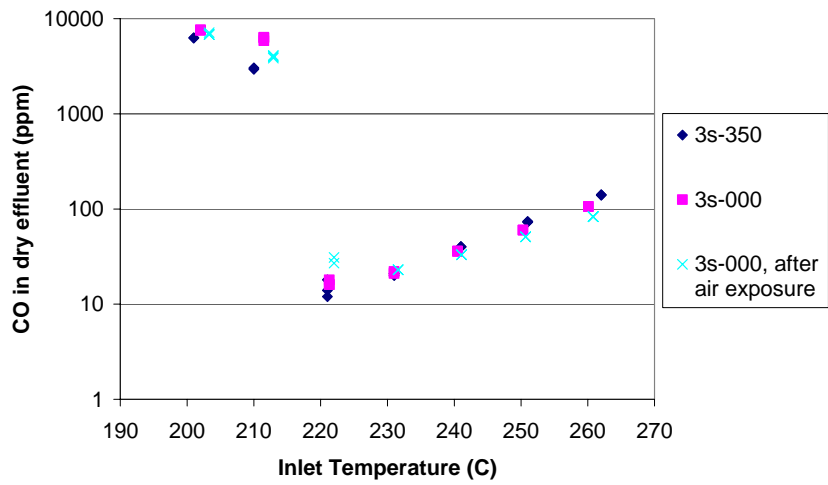
(A)
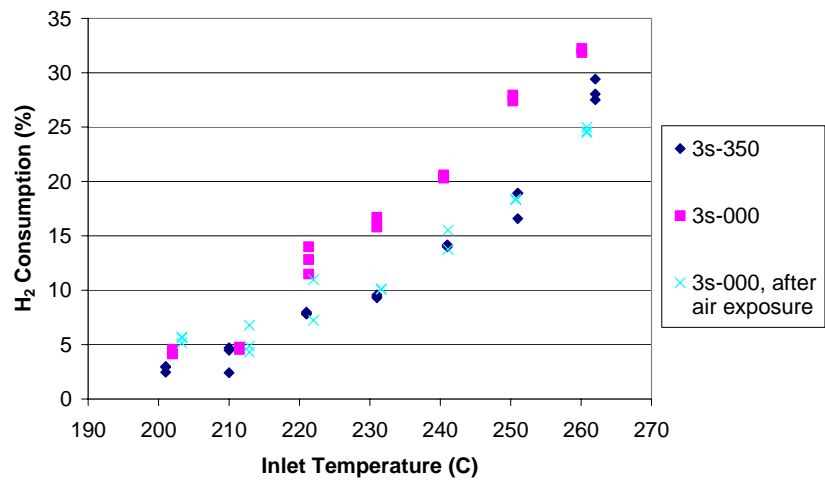


(B)

**Figure 15**: Effect of air exposure on a) CO concentration in the effluent and b) $H_2$ consumption (approximate feed composition: 0.9%CO, 24.5%$CO_2$, 68.9%$H_2$, 5.7%$H_2O$, SV=13,500 hr$^{-1}$).

## 5. Conclusions

In agreement with previous works, Pd/ZnO catalysts have been demonstrated as being selective for the methanol steam reforming reaction. This is due to the unique nature of the PdZn alloy formation upon reduction conditions higher than $>350^{\circ}$C. The presence of metallic Pd facilitates the methanol decomposition reaction. It has been shown that crystallite size may play an important role in determining the selectivity of the mechanism involved, even if the PdZn alloy is the predominant phase. For the unsupported catalysts, a crystallite size of ~8 nm was found to be optimum for minimal CO output. Using a high surface area alumina support greatly enhances the methanol steam reforming activity. Activities similar to that of a commercial CuZnAl catalyst were observed, under the same conditions. Metal loading as well as Pd:Zn ratio was found to be an important consideration. An optimum Pd:Zn ratio of 0.38 was found. Unlike their CuZnAl counterpart, PdZnAl catalysts are stable at much higher temperatures ($>280^{\circ}$C), and thus, the benefits of increased kinetics due to higher operating temperature are realized. Increasing the operating temperature from just $280^{\circ}$C to $310^{\circ}$C results in an almost 3-fold reaction rate increase.

The performance of selective CO methanation catalysis is markedly affected by metal loading, pretreatment, and reduction parameters. It was shown that a high surface area support is required for adequate CO activity. However, the crystallite size should be controlled, and actually increased, to suppress $CO_2$ methanation. These carefully controlled conditions result in a highly active and selective CO methanation catalyst. Under the conditions of this study, operating at high throughputs of SV=13,500 hr$^{-1}$, the

3%Ru metal loading catalyst with 350$^{o}$C reduction catalyst yielded a CO output less than 100 ppm over a temperature range from 240 $^{o}$C to 285 $^{o}$C, while not  exceeding a hydrogen consumption of 10%.   A selective CO methanation catalyst has been successfully developed as a viable option for CO removal in portable fuel processing applications.

# References

[1] M. Krumpelt, T. Krause, J. Carter, J. Kopasz, S. Ahmed, *Catalysis Today*. **2002,** 77, 3-4.

[2] D. Palo, J. Holladay, R. Dagle, Y. Chin, Submitted to *Fuel Processing for Portable Power*.

[3] J. Holladay, E. Jones, M. Phelps, J. Hu, *Journal or Power Sources*. **2002,** 108, 21-27.

[4] G. Xia, J. Holladay, R. Dagle, E. Jones, Y. Wang, *Chemical Engineering and Technology* (in press).

[5] P. Urban, A. Funke, J. Muller, M. Himmen, A. Docter, *Applied Catalysis A: General*. **2001,** 221, 467.

[6] T. Utaka, T. Okanishi, T. Takeguchi, R. Kikuchi, K. Eguchi, *Applied Catalysis A: General*. **2003**, 245, 343.

[7] N. Iwasa, S. Kudo, H. Takahashi, S. Masuda, N. Takezawa, *Catal. Lett*. **1993**, 19, 211.

[8] N. Iwasa, S. Masuda, N. Ogawa, N. Takezawa, *Catalysis Today*. **1997,** 36, 45-56.

[9] Y. Chin, R. Dagle, J. Hu, A. Dohnalkova, Y. Wang, *Catal Today*. **2002**, 77, 79.

[10] C. Weeler, A. Jhalani, E Klein, S. Tummala, L. Schmidt, *Journal of Catalysis*. **2004**, 223, 199.

[11] Y. Chin, R. Y. Wang, R. Dagle, X. Li. Li, *Fuel Processing Tech*. **2003**, 1681, 1.

[12] C. Cao, G. Xia, J. Holladay, E. Jones, Y. Wang, *Appl Catal. A: Gen*. **2004**, 262, 19.

[13] G. Hoogers, *Fuel Cell Technology Handbook*. **2003,** 5-12–5-14.

[14] C. Song, *Catalysis Today*. **2002,** 77, 41.

[15] P. Snytnikov, V. Sobyanin, V. Belyaev, P. Tsyrulnikov, N. Shitova, D. Shlyapin, *Applied Catalysis A: General*. **2003,** 239, 149.

[16] P. F. Joensen, J. Rostrup-Nielsen, *Journal of Applied Power Sources*. **2002,** 105, 199.

[17] M. Twigg, *Catalyst Handbook*, 2nd ed., **1997,** 350.

[18] L. Pettersson, R. Westerholm, *International Journal of Hydrogen Energy*. **2001,** 26, 255-256.

[19] B. Baker, J. Huebler, H. Linden; J. Meek, US Patent 3,615,164. **1971**.

[20] A. Rehmat, S. Randhava, ,*Ind. Eng. Chem. Res. Develop.,* **1970,** Vol 9, No. 4, 512-515.

[21] G. Bohm, T. Staneff, J. Steinwandel, US Patent 5,904,913. **1999.**

[22] V. Keulen, US Patent 6,407,307. **2001.**

[23] K. Otsuka, S. Takenaka, T. Shimizu, *International Journal of Hydrogen Energy*. **2004,** 29, 1065-1073.

[24] J. Holladay, Y. Wang, E. Jones, *Chemical Reviews*. **2004,** 104, 4767-4790.

[25] M. Muhler, J. Abmann, E. Loffler, A. Birkner, *Catalysis Today*. **2003,** 85, 235.

## Appendix 1

To depict the reproducibility of the activity data, below are the results for a catalyst twice run under identical conditions.
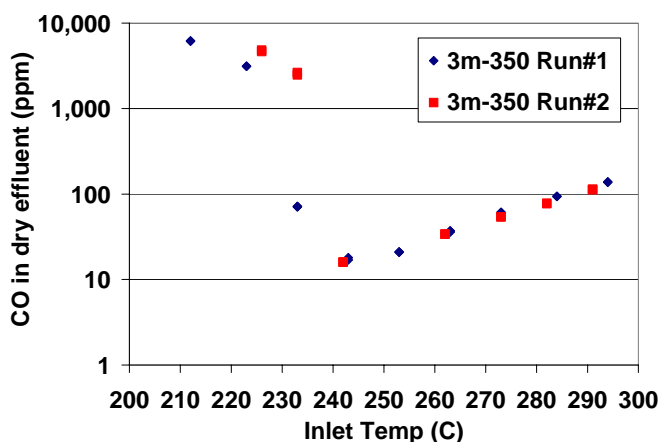
(A)
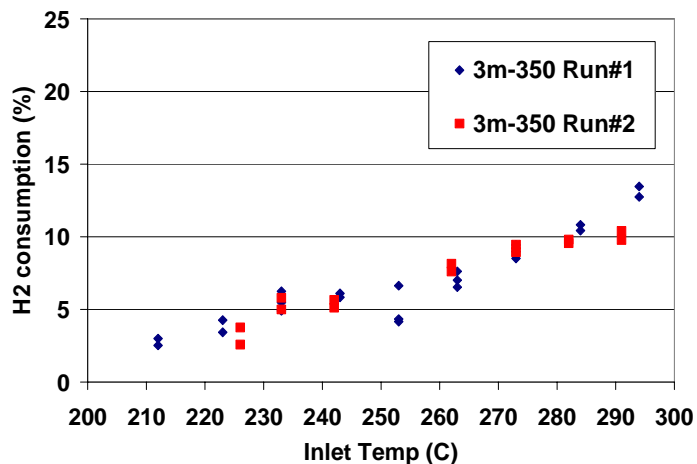
(B)

**Appendix 1**:  To depict the reproducibility of the data, included is an activity comparison of a catalyst twice run under identical conditions.  Results include a) CO concentration in the effluent and b) $H_2$ consumption (approximate feed composition:  0.9%CO, 24.5%$CO_2$, 68.9%$H_2$, 5.7%$H_2O$, SV=13,500 $hr^{-1}$).

**Appendix 2**

Appendix 2 is included in order to depict the accuracy of the methods used to determine the mean crystallite size found in Figure 6. From each TEM picture, as described in section 3.2, a plot of the crystallite size versus number of counts was made. From this histogram, a statistical analysis of the mean crystallite size was determined. From this analysis, the found mean crystallite size was plotted as a function of CO selectivity (Figure 6). One such histogram is shown below in Appendix 2a. Also included in Appendix 2b is the mean crystallite size plotted as a function of CO selectivity (similar to Figure 6), including the 95% confidence intervals. The error bars depict the range, that within at least 95% certainty, the mean crystallite size exists.
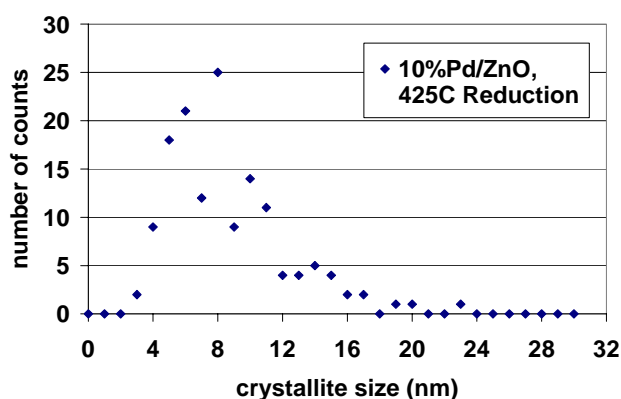


(A)
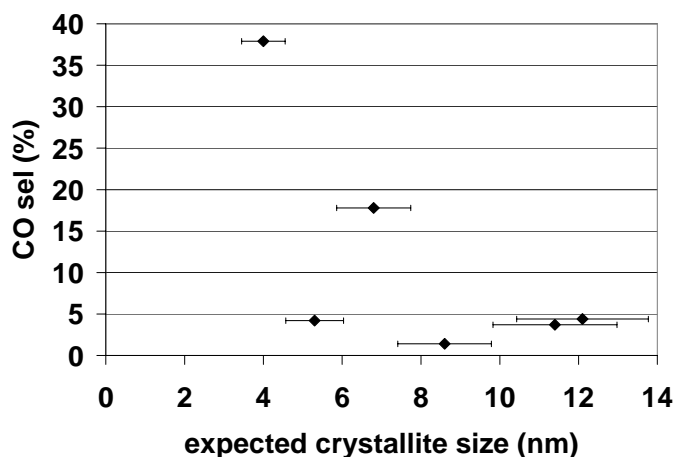


(B)

**Appendix 2**: a) Histogram of the crystallite size counts for the 10%Pd/ZnO catalyst reduced at 425$^{o}$C: number of counts versus crystallite size. b) CO selectivity versus crystallite size (similar to Figure 6) including approximate 95% confidence intervals. Within each range exists the mean crystallite size within at least 95% confidence.